

Article

Soft Computing and Machine Learning-Based Models to Predict the Slump and Compressive Strength of Self-Compacted Concrete Modified with Fly Ash

Dilshad Kakasor Ismael Jaf 

Engineering Department, College of Engineering, Salahaddin University, Erbil 44002, Iraq; dilshad.jaf@su.edu.krd

Abstract: Self-compacted concrete (SCC) is a special type of concrete; it is a liquid mixture appropriate for structural elements with excessive reinforcement without vibration. SCC is commonly produced by increasing the paste volume and cement content. As cement production is one of the huge factors in releasing CO₂ gas into the atmosphere, by-product materials such as fly ash are utilized as a cement replacement in concrete. In addition to the positive environmental impact, fly ash can maintain an excellent fresh and mechanical property. Incorporating fly ash into self-compacted concrete is widely applied in practice. However, its application is frequently limited by a lack of knowledge about the mixed material gained from laboratory tests. The most significant mechanical property for all concrete types is compressive strength (CS); also, the slump flow diameter (SL) in the fresh state is a crucial property for SCC. Hence, developing an accurate and reliable model for predicting the CS and SL is very important for saving time and energy, as well as lowering the cost. This research study proposed a projection of both the CS and SL of SCC modified with fly ash by three different model approaches: Nonlinear regression (NLR), Multi-Linear regression (MLR), and Artificial Neural Networks (ANN). In this regard, two different datasets were collected and analyzed for developing models: 308 data samples were used for predicting the CS, and 86 data samples for the SL. Each database included the same five independent parameters. The ranges for CS prediction were: cement (134.7–583 kg/m³), water-to-binder ratio (0.27–0.9), fly ash (0–525 kg/m³), sand (478–1180 kg/m³), coarse aggregate (578–1125 kg/m³), and superplasticizer (0–1.4%). The dependent parameter (CS) ranged from 9.7 to 81.3 MPa. On the other hand, the data ranges for the SL prediction included independent parameters such as cement (83–733 kg/m³), water-to-binder ratio (0.26–0.58), fly ash (0–468 kg/m³), sand (624–1038 kg/m³), coarse aggregate (590–966 kg/m³), and superplasticizer (0.087–21.84%). Also, the dependent parameter (SL) ranged from 615 to 800 m. Various statistical assessment tools, such as the coefficient of determination (R²), Root Mean Squared Error (RMSE), Mean Absolute Error (MAE), Objective value (OBJ), and Scatter Index (SI), were used to evaluate the performance of the developed models. The results showed that the ANN model best predicted the CS and SL of SCC mixtures modified with fly ash. Furthermore, the sensitivity analysis demonstrated that the cement content is the most effective factor in predicting the CS and SL of SCC mixtures.



Citation: Ismael Jaf, D.K. Soft Computing and Machine Learning-Based Models to Predict the Slump and Compressive Strength of Self-Compacted Concrete Modified with Fly Ash. *Sustainability* **2023**, *15*, 11554. <https://doi.org/10.3390/su151511554>

Academic Editor: Ahmed Salih Mohammed

Received: 2 July 2023

Revised: 14 July 2023

Accepted: 17 July 2023

Published: 26 July 2023

Keywords: self-compacting concrete; mix proportion; slump flow; compressive strength; modeling



Copyright: © 2023 by the author. Licensee MDPI, Basel, Switzerland. This article is an open access article distributed under the terms and conditions of the Creative Commons Attribution (CC BY) license (<https://creativecommons.org/licenses/by/4.0/>).

1. Introduction

Self-compacted concrete (SCC) is one of the special types of concrete with a high viscosity without any requirement for compaction. SCC is vital in the concrete industry due to its numerous benefits. The main idea of SCC is to increase the amount of paste volume to increase the rheological property of the mixture. Thus, the SCC can spread completely inside the formwork by its weight without any bleeding or segregation. Thus, the labor cost will be eliminated. However, utilizing excessive cement leads to a higher cost of SCC production [1–3]. SCC is an excellent choice for congestion structural elements due to its high flowability. The high flowability and stability of SCC can be achieved by utilizing

different mineral and chemical admixtures; fly ash and superplasticizer, respectively, are commonly used [4]. Fly ash is one of the common replacements for cement in concrete. It can provide lower costs by reducing the utilization of cement and improving the mixture's flowability due to its rounded shape. One of the advantages of SCC over the other special concretes is that SCC does not require any special curing method; the same methods and procedures for normal concrete can also be used for SCC [5].

In the fresh state, the slump flow diameter (SL) of SCC is an important property that should be checked. Also, among the mechanical properties in the hardened state, the compressive strength (CS) of SCC is one of the significant parameters in the design of engineering structures. Other mechanical properties and the durability of SCC have a direct or indirect relation to compressive strength, and they can be derived from the CS [6,7].

The term 'water-to-binder ratio' (w/b) refers to the ratio of water to cement plus pozzolanic material. One of the most common and most-well known pozzolanic materials is fly ash, which has been used to improve some significant properties of self-compacted concrete, such as workability. The compressive strength of SCC is improved by increasing the water-to-binder ratio [8]. Karamoozian et al. [9] noticed that, for the same water content, increasing the cement content from 360 to 450 kg/m³ increased the compressive strength of SCC from 48 to 52 MPa at 28 days of curing. Similar findings have been reported in other studies [10,11]. The w/b is one of the significant factors influencing the compressive strength of SCC, similar to normal concrete. For SCC, the ratio is normally lower than normal concrete. A lower w/b refers to lower water content and a higher amount of binder materials, leading to a higher CS and a more homogeneous matrix. Ahmadi et al. [12] stated that the w/b ratio has a greater impact on the compressive strength of normal concrete than on the self-compacting compressive strength. Naderpour and Abbasi [13] investigated the effect of different w/b ratios on the compressive strength of SCC. It was noticed that lowering the w/b ratio from 0.45 to 0.35 improved the CS of SCC at all curing ages (from 3 to 56 days).

Since the volume of aggregates in the SCC is about 60–70% of its total volume, aggregate greatly influences the rheological and mechanical properties of SCC. Compared to conventional concrete, lower coarse aggregate content is utilized in the production of SCC [1,3,14]. The study by [15] showed that the coarse aggregate had a greater impact on the CS of SCC than the fine aggregate content. However, the fine aggregate has more influence on the homogeneity and viscosity of the SCC mixture [16].

In addition to adding pozzolanic materials, SCC production is impossible without superplasticizers. This is due to the utilization of high cement and binder content in SCC. Therefore, high workability (slump flow diameter) can be achieved in SCC only when the SP content is increased. Adding SP to the SCC mixture improves the rheological performance but has different effects on the compressive strength based on the SP dosage. A previous study by Sor N. A. [17] concluded that increasing the SP dosage from 5.5 kg/m³ to 8.25 kg/m³ increased the compressive strength of SCC from 35 MPa to 45.5 MPa at 28 days.

As illustrated above, the compressive strength of SCC is sensitive and affected by several parameters. Therefore, apart from experimental work in the laboratory, which is quite costly, it is important to utilize more advanced techniques to predict the CS value through various statistical tools and numerical equations. Soft computing techniques [18–22] are currently one of the most common and ideal approaches for predicting measured values; they may be a good alternative for solving linear or nonlinear problems where mathematical models cannot simply indicate the relationship between the involved parameters in the problem [23]. Mohammed et al. [24] created a systematic multiscale model to predict the CS of fly ash-based concrete. A total of 450 experimental data were used for modeling in their study. For the qualifications, the Linear regression (LR), Nonlinear regression (NLR), Multi-Linear regression (MLR), M5P-tree, and Artificial Neural Network (ANN) models were all developed. It was concluded that the MLR, M5P-tree, and ANN models were the

most accurate and reliable in predicting the CS of high-volume fly ash concrete, with higher R^2 values and lower RMSE and MAE values.

In this study, two different databases of fly ash-based self-compacted concrete mixtures with the same parameters were prepared. The first database consisted of 308 data samples of SCC mixtures, and it was used to predict the compressive strength; the second one had 86 data points used to predict the slump flow diameter of SCC. Thus, the CS and SL are were dependent parameters predicted independently using collected databases. The independent parameters of SCC were in various ranges, which included cement (C), water-to-binder ratio (w/b), fly ash (FA), sand (S), coarse aggregate (CA), and superplasticizer (SP).

As fly ash has a wide range of applications for producing SCC mixtures, a reliable and accurate model cannot be found in the literature regarding the efficient use of FA in SCC mixtures for the construction industry. As a result, this study attempted to evaluate and quantify the effect of a wide range of mixture proportions on the CS and SL of SCC, including the cement content (kg/m^3), water-to-binder ratio, fly ash content (kg/m^3), sand content (kg/m^3), coarse aggregate content (kg/m^3), and superplasticizer percentage amount.

Three different model techniques, namely NLR, MLR, and ANN, were performed to predict the CS [25–28] and SL of SCC modified with FA using the databases collected from the literature. Furthermore, the most accurately developed model was applied to different CS and SL ranges. The compressive strength ranges were as follows: low-strength concrete (LSC), lower than 20 MPa; Normal-strength concrete (NSC), between 20 and 55 MPa; and High-strength concrete (HSC), CS greater than 50 MPa [29]. The slump flow diameter was divided into three different classes: the SL from 550 to 650 mm (Class 1), SL between 650 and 750 mm (Class 2), and SL of greater than 750 mm (Class 3) [5]. In addition, different assessment criteria, such as the Correlation Coefficient (R^2), Mean Absolute Error (MAE), Root Mean Squared Error (RMSE), Objective (OBJ), and Scatter Index (SI), were used to evaluate the performance of the developed models.

Research Objectives

This study aims to evaluate the effect of fly ash on the compressive strength and slump flow diameter of self-compacted concrete mixtures collected from literature; the following are the main objectives:

- I. Perform statistical analysis to determine the influence of concrete ingredients, such as the cement, water-to-binder ratio, fly ash, sand, coarse aggregate, and superplasticizer, on self-compacted concrete's compressive strength and slump flow diameter.
- II. Provide a systematic multiscale model and propose to predict the compressive strength and slump flow diameter of self-compacted concrete containing up to 70% of fly ash, with a variety of cement, sand, and coarse aggregate content, as well as different water-to-binder ratios and superplasticizer percentages.
- III. Apply the most accurately developed model on different compressive strength ranges and slump flow diameter classes.
- IV. As an alternative to the developed model techniques (NLR, MLR, and ANN), determine the most reliable and accurate model based on different statistical assessment criteria to predict the CS and SL of fly ash-based self-compacted concrete.
- V. The overall and main objective of the current study is to model compressive strength as one of the significant mechanical properties of concrete and slump flow diameter as a fresh state property of SCC modified with different FA content.

2. Methodology

2.1. Data Collection

Two databases were prepared for each targeted parameter to develop a reliable and applicable model to predict both the compressive strength and slump flow diameter of self-compacted concrete modified with fly ash. The independent parameters included six main

parameters: cement content (kg/m^3), water-to-binder ratio, fly ash content (kg/m^3), sand (kg/m^3), coarse aggregate (kg/m^3), and superplasticizer (%). For the compressive strength and slump flow, 308 data samples [30–51] and 86 data samples [31,37,38,41,42,50–63] were selected, respectively, as shown in Table 1. According to the literature [29,64–66], the datasets were divided into two groups, training (by 70%) and testing (by 30%), using the Rand Function. The training dataset included 216 samples for CS data, while the testing data included 92 samples to check the validity of the developed models based on the training datasets. The training and testing datasets for the SL database were determined as 60 samples and 26 samples, respectively. Figure 1 shows the methodology of the current study.

Table 1. Summary of collected data for CS and SL prediction in FA-modified SCC.

References	Cement, C (kg/m^3)	Water-to-Binder Ratio (w/b)	Fly Ash, FA (kg/m^3)	Sand, S (kg/m^3)	Coarse Aggregate, CA (kg/m^3)	Superplasticiz SP (%)	Compressive Strength, CS (MPa)
[30]	134.7–540	0.27–0.9	0–525	487–1135	600–1125	0–1.36	9.74–79.19
[31]	160–280	0.34–0.45	120–240	808–1034	900	0.1–0.6	31–52
[32]	280–400	0.55–0.87	0–120	718–1042	850	0.12–0.75	13.3–41.2
[33,34]	183–317	0.38–0.65	100–261	478–919	837	0–1	Oct-43
[35]	533–583	0.31–0.33	50–215	813–835	745–766	0.24–0.46	50–81
[36]	161–247	0.35–0.45	159–254	842–866	843–864	0–0.4	26.2–38.0
[37]	250–427	0.31–0.59	90–257	768–988	659–923	0.09–0.9	47–66
[38]	220–440	0.32	110–330	686–714	881–917	0.62–0.69	48–70
[39]	300–350	0.38–0.4	150–200	830–845	860–876	0.818–0.827	21.6–26.5
[40]	380	0.38	20	1180	578	0.398	40.4
[41]	275–350	0.34–0.36	150–325	611–707	777–901	0.795–1.25	50–72
[42]	165–275	0.37–0.58	275–385	735–796	865–937	0.836–0.74	37.92–63.32
[43]	215	0.38	215	925	905	0.15	20.4
[44]	290	0.38	290	975	650	0.45	37.97
[45]	300	0.28	300	787	720	0.33	52.7
[46]	420	0.33	80	785	860	0.3	56
[47]	350	0.35	150	900	600	1.0	37.18
[48]	360	0.28	240	853	698	0.3	63.5
[49]	344–399	0.35	100–147	814	881–882	0.116–0.146	48.75–55
[50]	225	0.35	275	908	652	0.70	41.42
[51]	480	0.38	96	819	699	0.94	53
References	Cement, C (kg/m^3)	Water-to-binder ratio (w/b)	Fly ash, FA (kg/m^3)	Sand, S (kg/m^3)	Coarse aggregate, CA (kg/m^3)	Superplasticiz SP (%)	Slump flow diameter, SL (mm)
[52]	450–480	0.40–0.45	0–144	890	810	4.8–13.3	650–695
[50]	500	0.35	0–275	908–967	652–694	0.7–8	630–700
[37]	220–427	0.31–0.41	90–330	686–988	659–923	0.18–0.9	670–749
[38]	550	0.32–0.44	0–110	728–826	855–935	3.2–8.43	670–675
[53]	530	0.45	0–265	768	668	0.09–4.55	660–690
[41]	83–385	0.31–0.41	165–468	624–732	794–931	1–1.25	680–800
[31]	430–450	0.36–0.39	202.5–232.2	872–808	900	1.58–2.15	680–710
[54]	465–550	0.41–0.44	83–193	910	590	0.97–11	635–690
[55]	450–500	0.39–0.43	135–225	724–789	850–926	2.5–6.15	640–680
[56]	500	0.35	150–250	900	600	10.5–11	660–680
[57]	550	0.41–0.44	83–193	910	590	9.91–11.01	633–690
[58]	180–270	0.44	180–270	788–801	829–842	0.27–0.28	720–730

Table 1. Cont.

References	Cement, C (kg/m ³)	Water-to-binder ratio (w/b)	Fly ash, FA (kg/m ³)	Sand, S (kg/m ³)	Coarse aggregate, CA (kg/m ³)	Superplasticizer SP (%)	Slump flow diameter, SL (mm)
[42]	165–385	0.29–0.58	165–385	735–821	865–966	0.74–0.84	670–730
[59]	567–670	0.26–0.31	0–156	656–846	729–875	12.39–21.84	615–655
[60]	733	0.26	271.21	748	698	8.40	660
[49]	399	0.35	100	814	882	0.146	690
[61]	500	0.35	0	1038	639	6.75	665
[51]	480	0.38	96	819	699	0.94	680
[62]	437	0.34	80	743	924	0.43	700
[63]	321.75	0.36	173.25	862.45	729.18	0.545	696

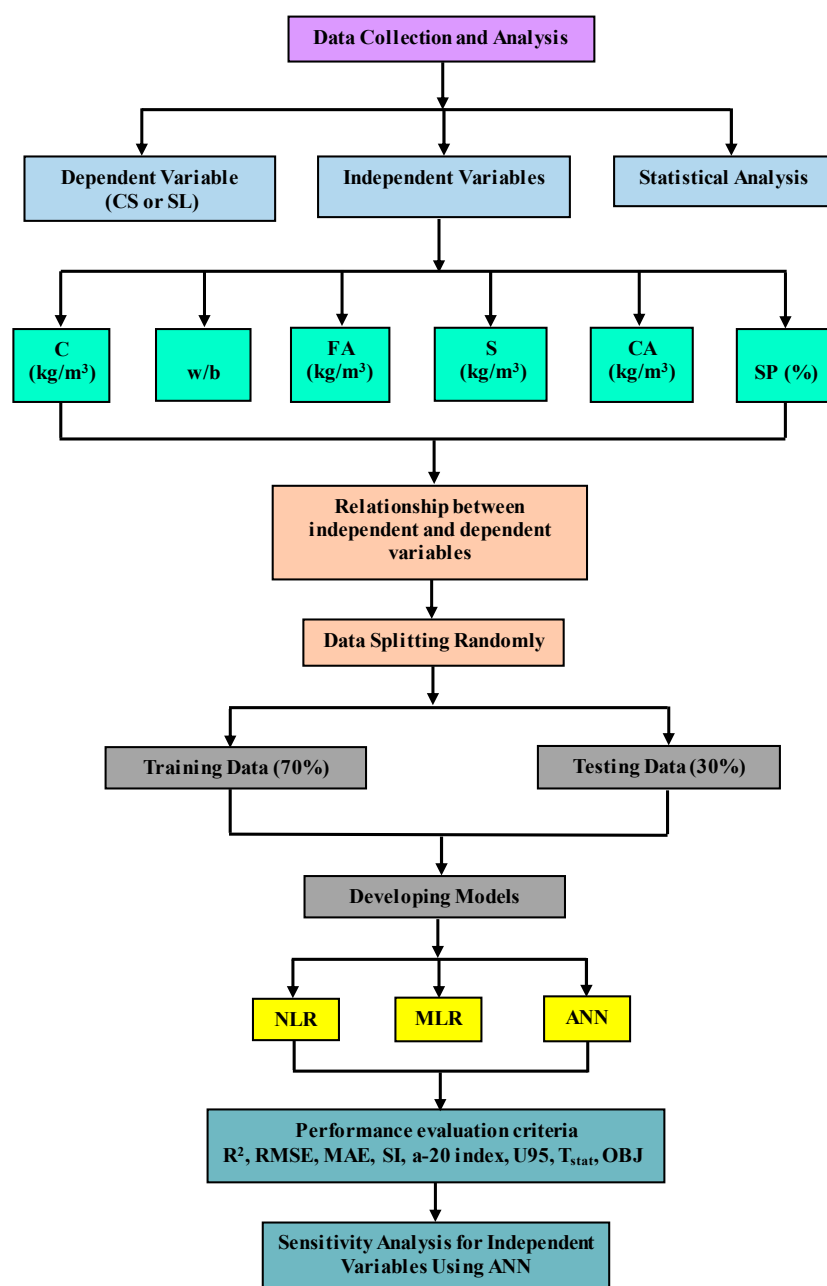


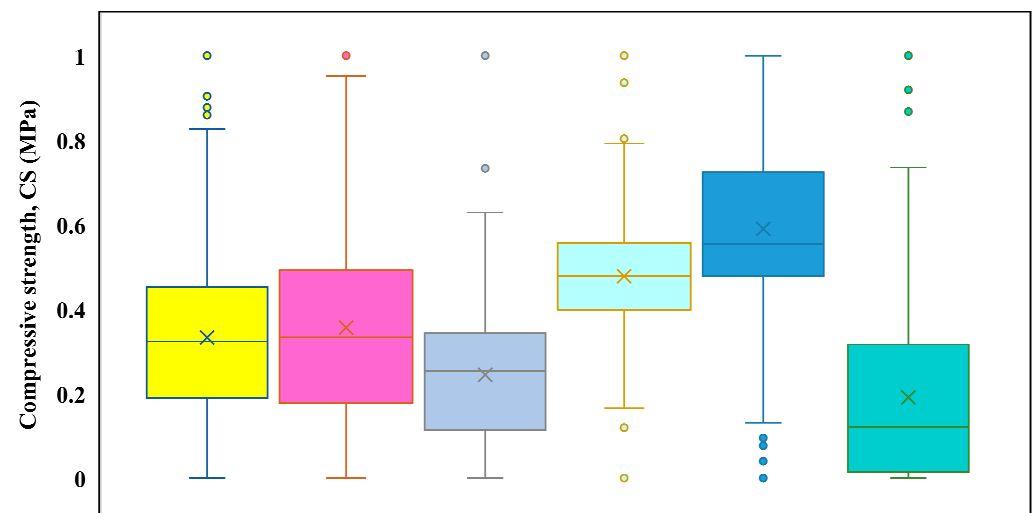
Figure 1. Flowchart of the study.

2.2. Pre-Processing

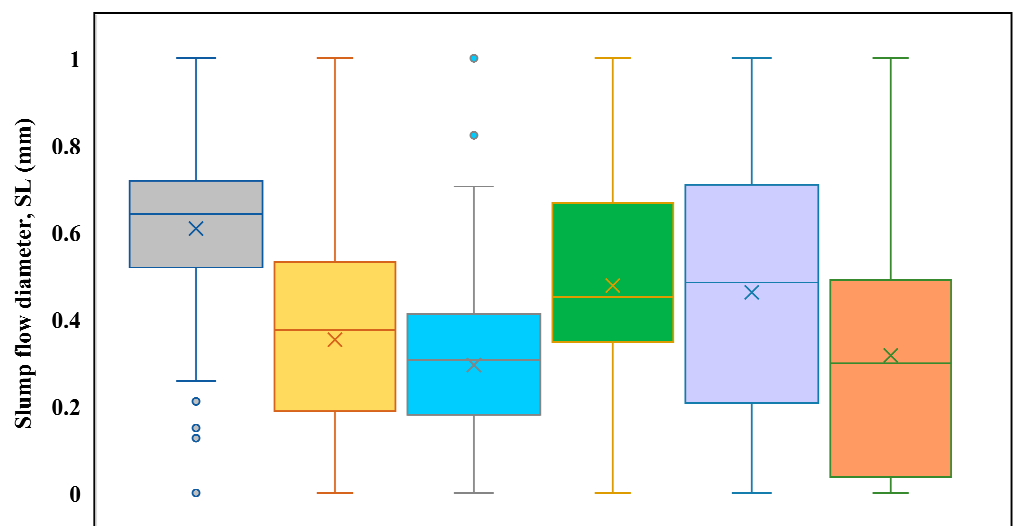
The pre-processing technique is a vital step before using a dataset. The process can improve the performance of created models. In the current study, each independent variable was converted to a value between zero and one utilizing Equation (1) [29,67]. The converted values in both the CS and SL databases are demonstrated in the box plot (Figure 2).

$$N_f = \frac{(N_i - N_{i\min})(N_{f\max} - N_{f\min})}{(N_{i\max} - N_{i\min})} + N_{f\min} \quad (1)$$

where N_i represents the old value and N_f represents the new value. The $N_{f\min}$ is zero and $N_{f\max}$ is one.



(a)



(b)

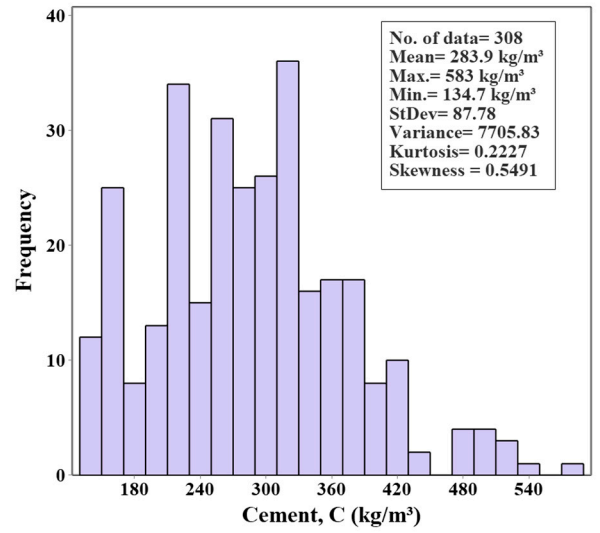
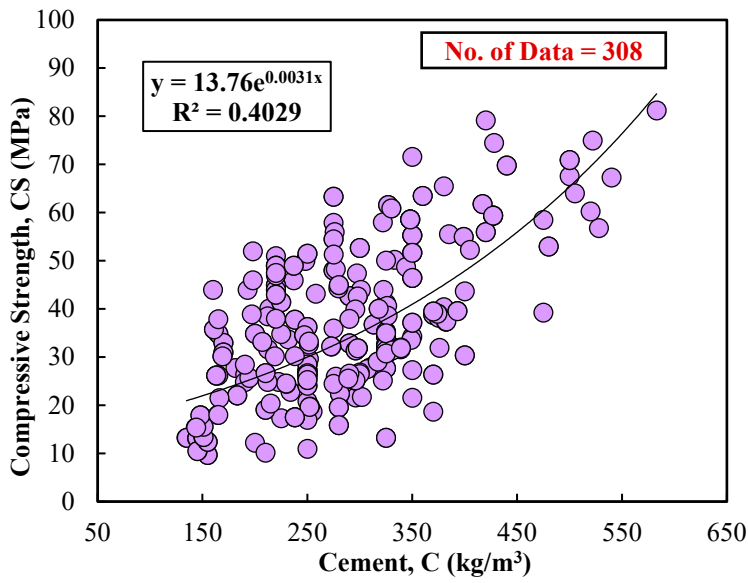
Figure 2. Box plot of the independent parameters in (a) the CS dataset and (b) the SL dataset.

2.3. Statistical Evaluation

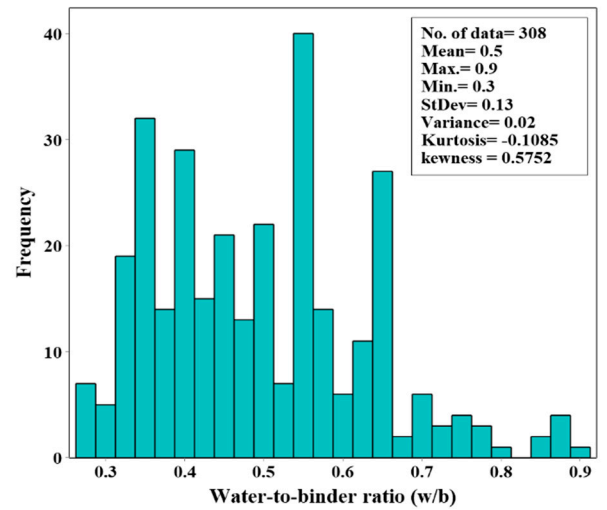
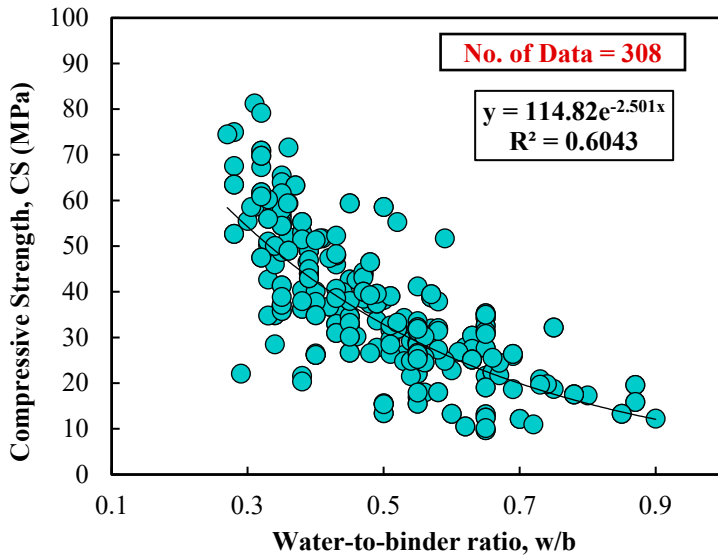
The data collected to predict the compressive strength and slump flow diameter of SCC mixtures were statistically analyzed to determine the relationship between each independent variable (C, w/b, FA, S, CA, and SP) with the dependent variables (CS and SL). In this regard, statistical functions such as Mean, Median, Mode, Standard Deviation (SD), Skewness (Skew), Kurtosis (Kur), Variance (Var), Maximum (Max), and Minimum (Min) were calculated. Skewness depicts the distribution of variables, whether positive or negative, on the right or left, with positive values on the right and negative values on the left. A negative value for kurtosis indicates a short distribution tail, whereas a positive value indicates a longer tail. The statistical analysis is summarized in Table 2 for both the CS and SL datasets. The histogram of each independent variable and its relationship with compressive strength and the slump flow are plotted in Figures 3 and 4, respectively.

Table 2. Summary of the statistical analysis of the FA-modified SCC parameters for the CS and SL prediction.

Compressive strength database	Variables	C (kg/m ³)	w/b	FA (kg/m ³)	S (kg/m ³)	CA (kg/m ³)	SP (%)	CS (MPa)
	Mean	283.9	0.5	128.3	813.5	900.7	0.3	36.6
	Median	279.8	0.5	133	813.5	881	0.2	34.5
	Mode	250	0.55	0	916	837	0	49
	SD	87.78	0.13	86.4	95.24	109.26	0.28	15.08
	Var	7705.83	0.02	7465.52	9070.26	11,937.73	0.08	227.5
	Kurt	0.2227	−0.1085	1.0307	2.2695	0.2755	0.9795	−0.2692
	Skew	0.5491	0.5752	0.4626	0.2461	−0.0674	1.1913	0.4736
	Min	134.7	0.27	0	478	578	0	9.7
	Max	583	0.9	525	1180	1125	1.4	81.3
Slump flow database	Variables	C (kg/m ³)	w/b	FA (kg/m ³)	S (kg/m ³)	CA (kg/m ³)	SP (%)	SL (mm)
	Mean	478.3	0.37	137.7	821.5	763.5	6.97	674.9
	Median	500	0.38	142.9	810.5	772	6.58	675
	Mode	550	0.35	0	910	590	4.55	680
	SD	122.18	0.065	91.65	82.42	113.97	5.94	31.52
	Var	14,928.1	0.00428	8399.5	6792.83	12,989.31	35.33	993.62
	Kurt	0.8148	−0.2208	1.2492	−0.5606	−1.2545	−0.5945	1.9597
	Skew	−0.8308	−0.0041	0.6296	0.0668	−0.1665	0.569	0.8086
	Min	83	0.26	0	624	590	0.087	615
	Max	733	0.58	468	1038	966	21.84	800

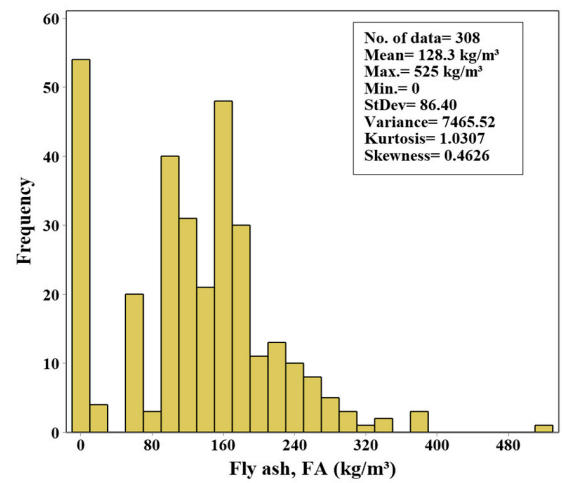
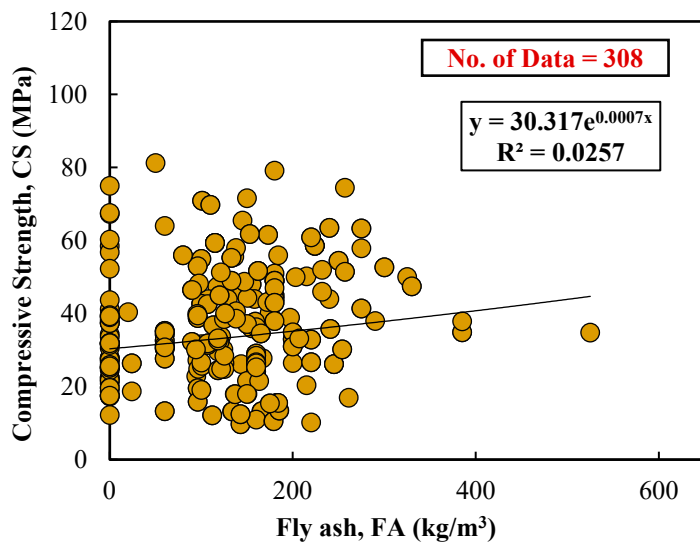


(a)

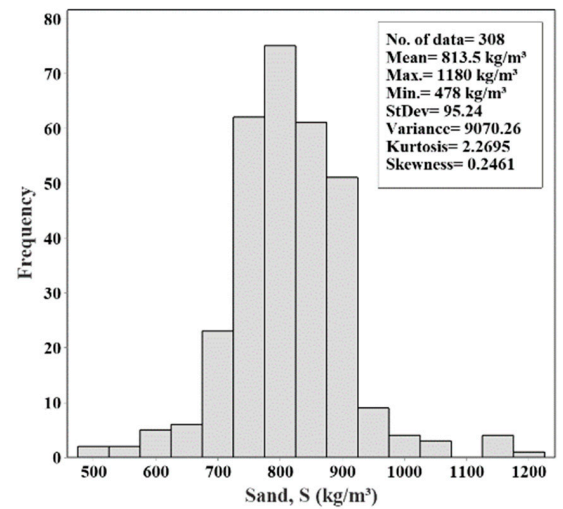
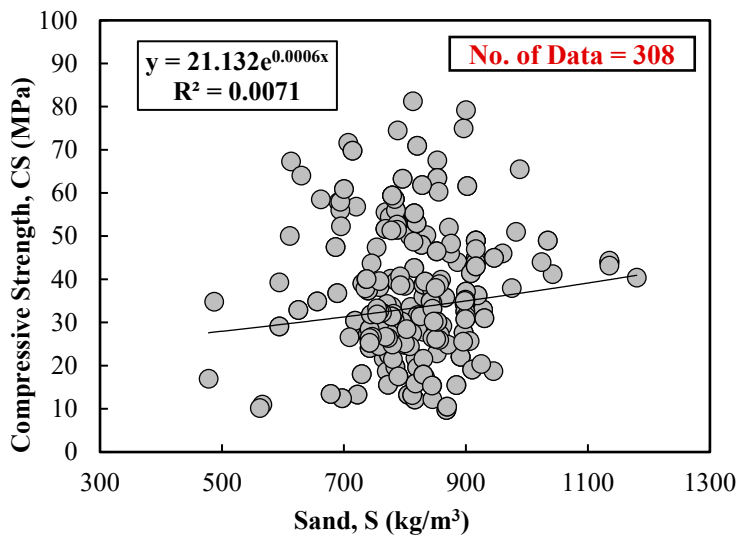


(b)

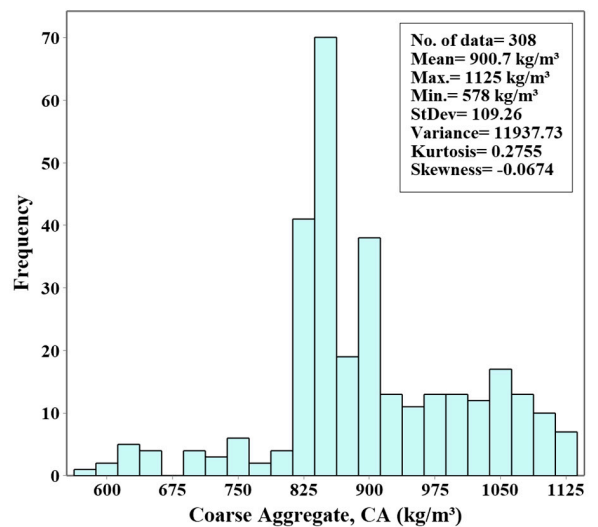
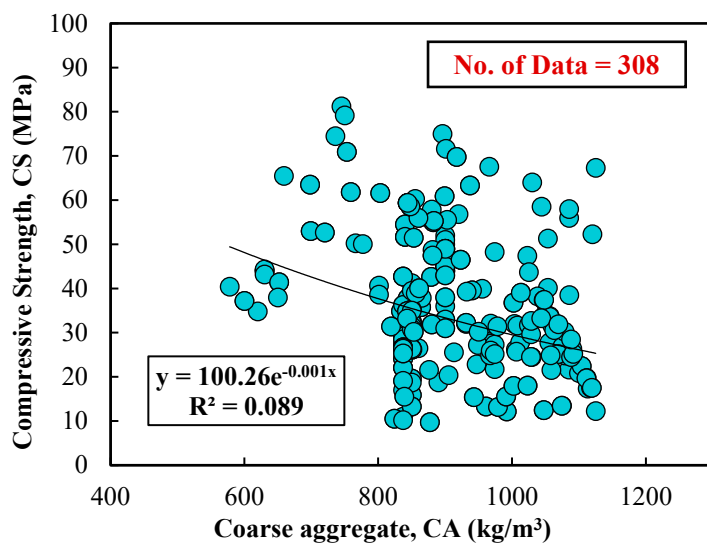
Figure 3. Cont.



(c)



(d)



(e)

Figure 3. Cont.

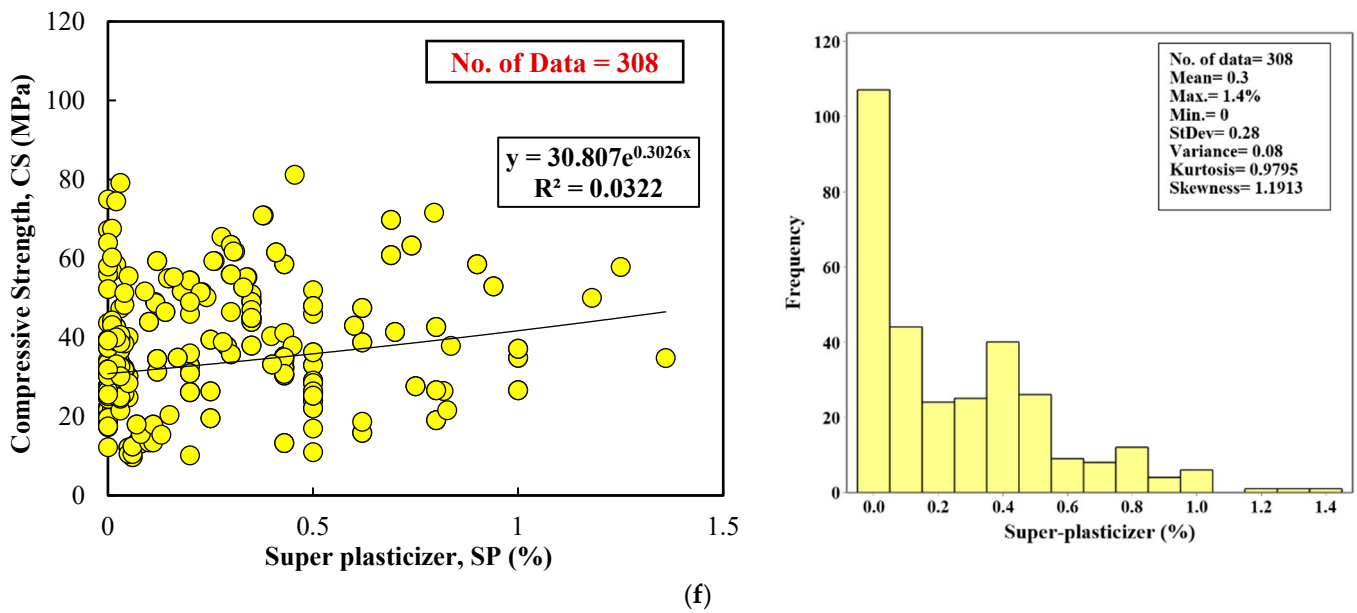


Figure 3. Histogram and Marginal plots for the compressive strength of FA-modified SCC with (a) cement (kg/m^3), (b) water-to-binder ratio, (c) fly ash (kg/m^3), (d) fine aggregate (kg/m^3), (e) coarse aggregate (kg/m^3), and (f) superplasticizer (%).

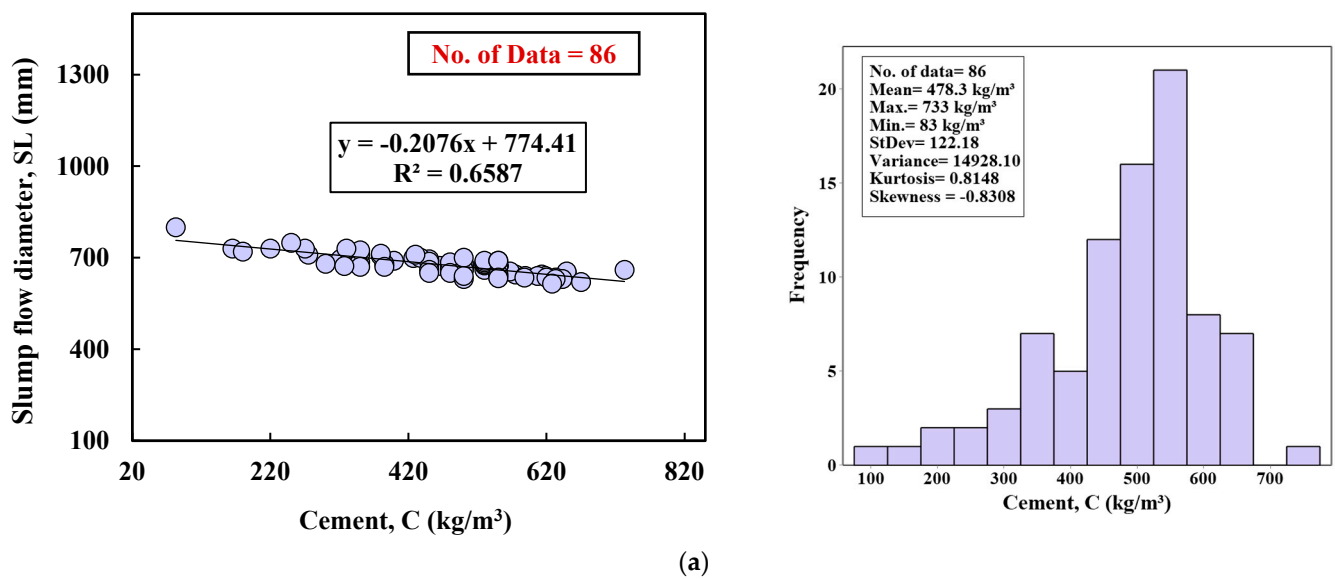
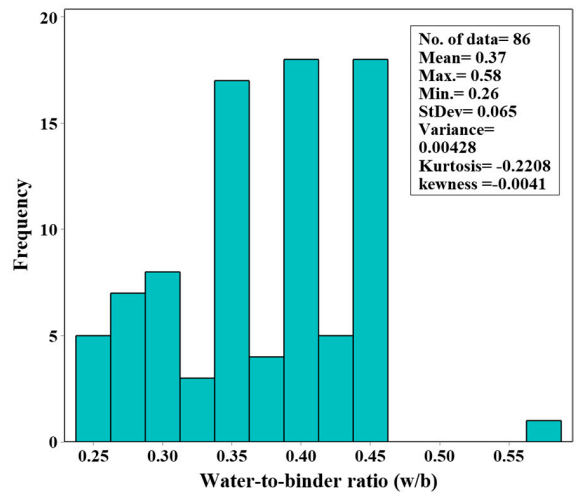
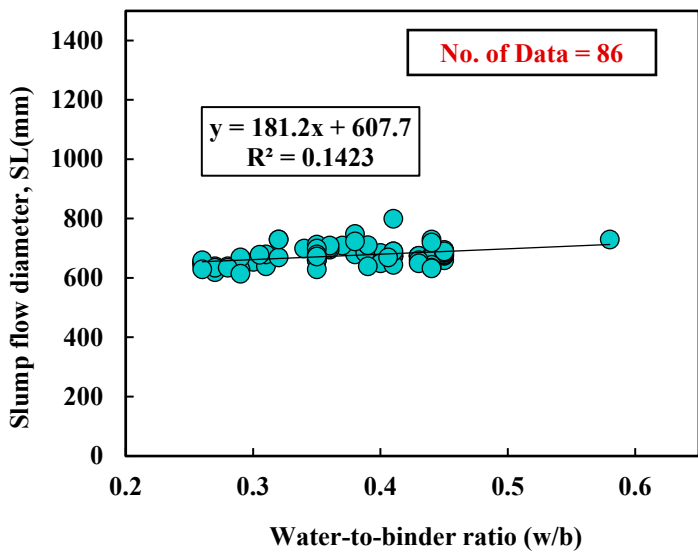
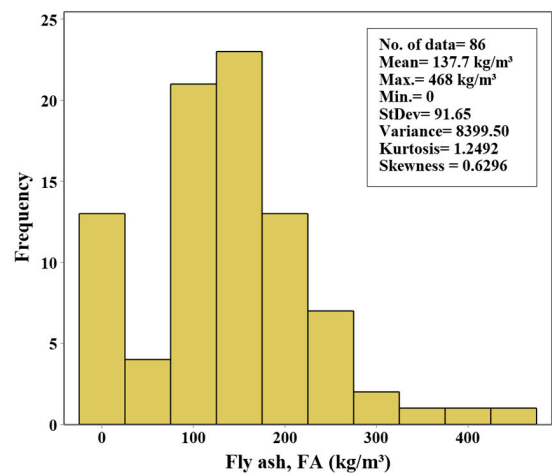
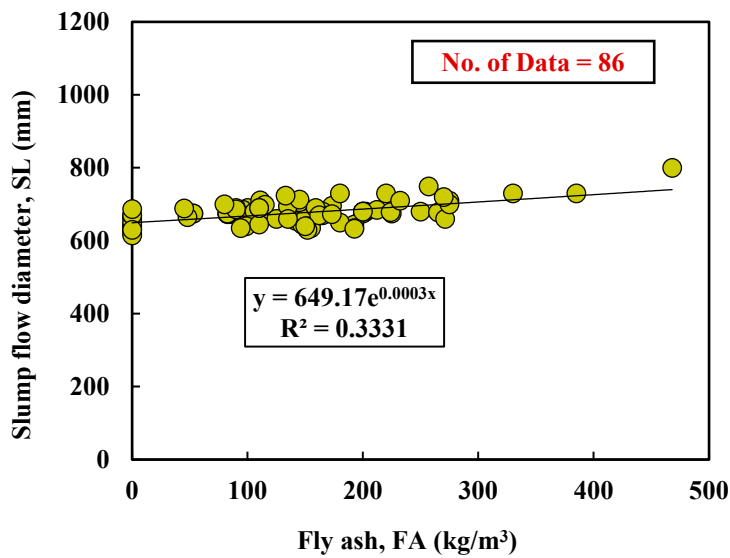


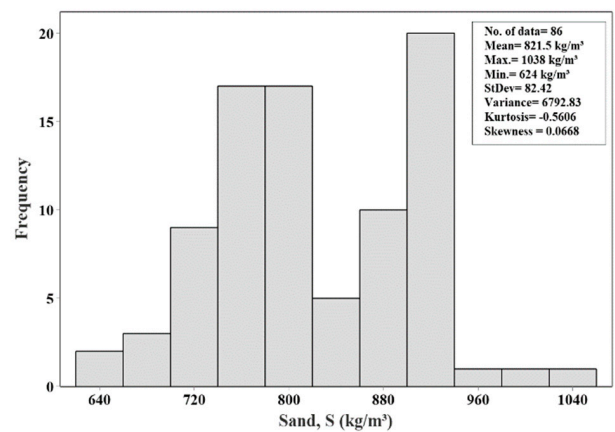
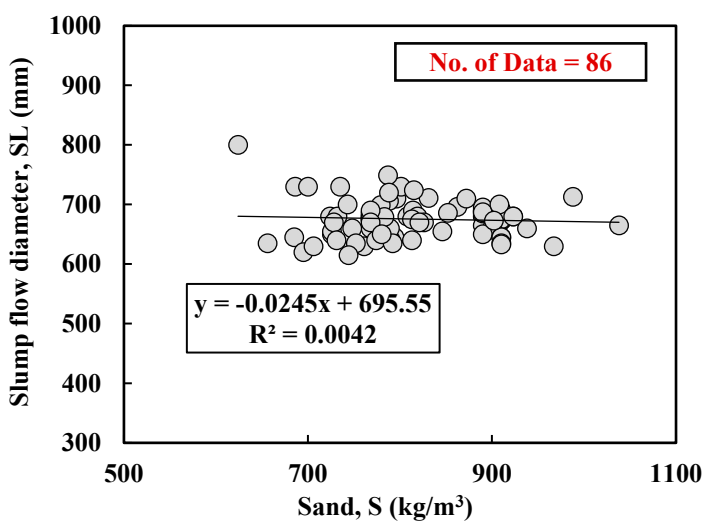
Figure 4. Cont.



(b)



(c)



(d)

Figure 4. Cont.

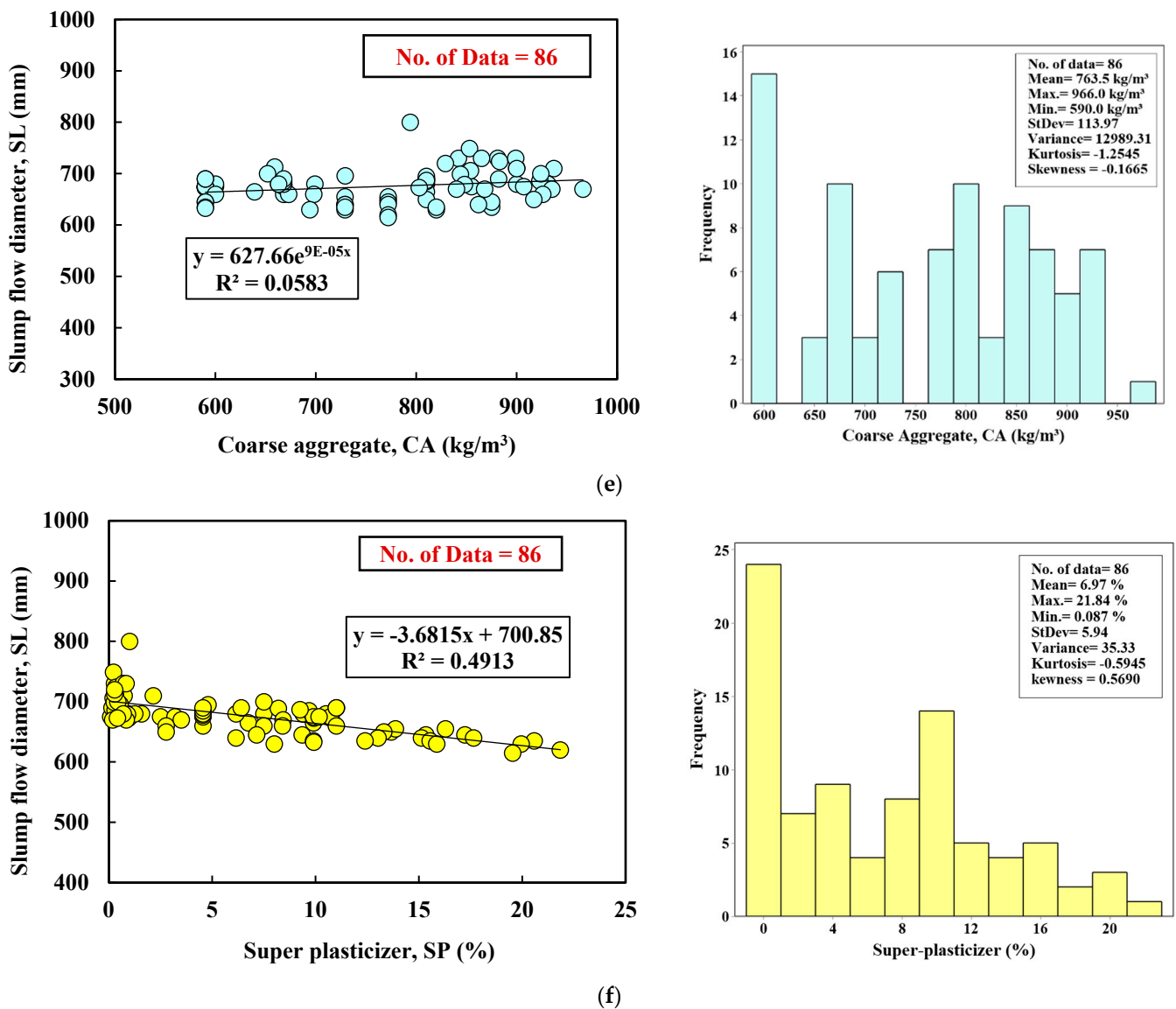


Figure 4. Histogram and Marginal plots for the slump flow diameter of FA-modified SCC with (a) cement (kg/m^3), (b) water-to-binder ratio, (c) fly ash (kg/m^3), (d) fine aggregate (kg/m^3), (e) coarse aggregate (kg/m^3), and (f) superplasticizer (%).

2.4. Modeling

As illustrated in Figure 5, the relationships between compressive strength or slump flow diameter and other compositions of FA-modified SCC mixtures, such as cement, water-to-binder ratio, fly ash, sand, coarse aggregate, and superplasticizer, were obtained. Based on the correlation matrix, a good correlation between cement and compressive strength was observed, which was 0.632. However, a poor correlation was noted for the other variables. The correlations were -0.748 , 0.161 , 0.082 , -0.301 , and 0.185 , respectively. On the other hand, the relationships between independent parameters and the slump flow diameter were determined. The highest correlation between the FA and the SL was 0.572. However, poor relationships were found between C, w/b, S, CA, SP, and SL. The relations were -0.814 , 0.397 , -0.052 , 0.236 , and -0.705 , respectively.

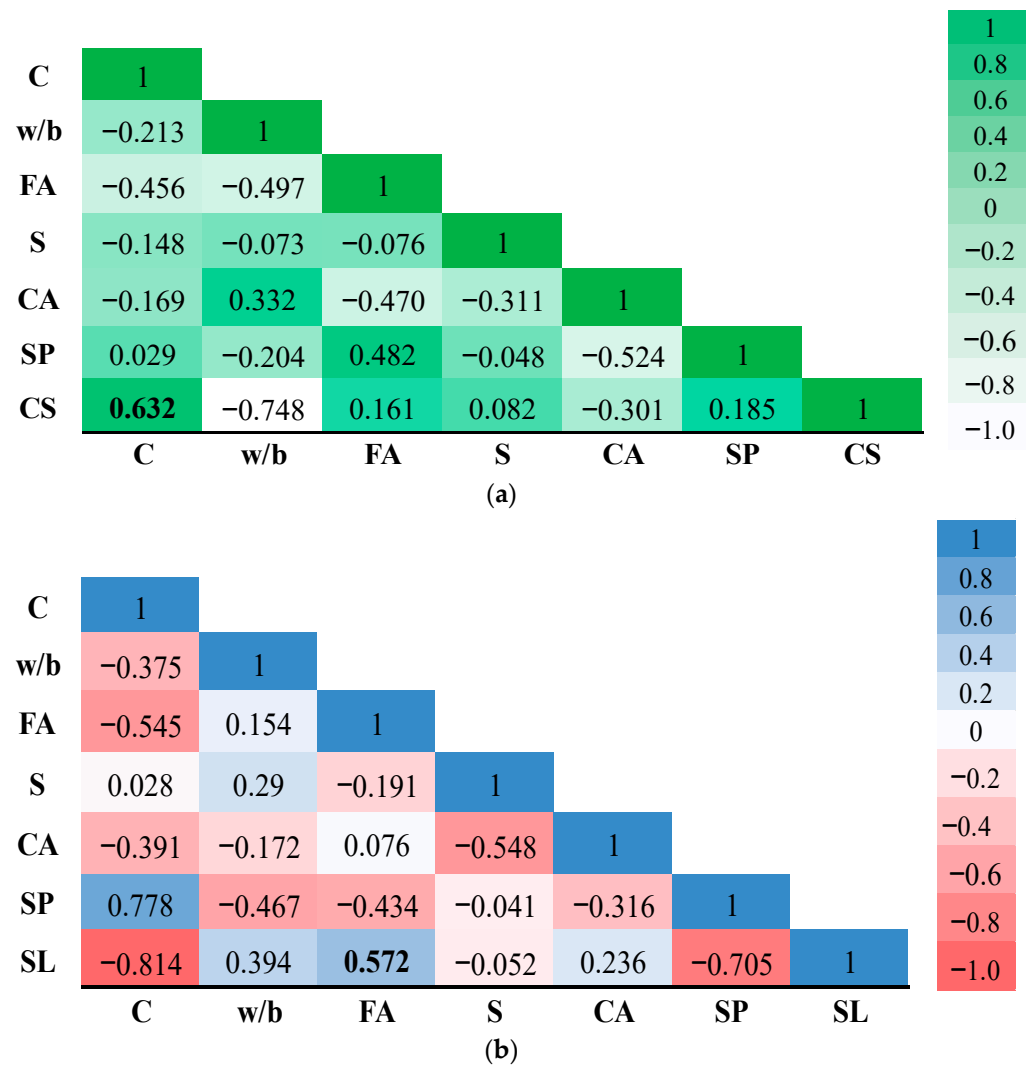


Figure 5. Correlation matrix plot between the dependent and independent variables of FA-modified SCC based on (a) CS and (b) SL.

Therefore, three models were proposed below to evaluate the effect of the various mixture proportions mentioned above on the CS and SL of SCC modified with FA. This study used NLR, MLR, and ANN models to predict the CS and SL of SCC mixtures. The most accurate and reliable model was proposed based on the following criteria: the model must be scientifically valid, with a lower percentage error between the measured and predicted data and a lower RMSE, MAE, OBJ, SI, and a higher R² value.

2.4.1. Nonlinear Regression (NLR) Model

Equation (2) can be used as a general form to develop a nonlinear regression model to determine [24,68] both the compressive strength and slump flow diameter, including the fly ash content and the self-compacted concrete components. The model was developed for each dependent parameter independently using the mentioned collected database. NLR is an advanced representation of the MLR model that is accurate and reliable. However, the model has a disadvantage in the form of mathematical complications [69].

$$CS, SL = \alpha_1(C)^{\alpha_2} + \alpha_3(w/b)^{\alpha_4} + \alpha_5(FA)^{\alpha_6} + \alpha_7(S)^{\alpha_8} + \alpha_9(CA)^{\alpha_{10}} + \alpha_{11}(SP)^{\alpha_{12}} \quad (2)$$

where $\alpha_1, \alpha_2, \alpha_3 \dots \alpha_{11}$ and α_{12} are the model parameters. CS, SL, w/b, FA, S, CA, and SP are the compressive strength (MPa), slump flow diameter (mm), cement (kg/m³), water-to-

binder ratio, fly ash (kg/m^3), sand (kg/m^3), coarse aggregate (kg/m^3), and superplasticizer (%), respectively.

2.4.2. Multi-Linear Regression (MLR) Model

The Multi-Linear Regression model can predict the compressive strength and slump flow diameter of the fly ash-modified self-compacted concrete with different mix design components. The equation of MLR includes the product of significant parameters affecting the CS and SL of the self-compacted concrete in exponential and constant terms (Equation (3)). The MLR model has several advantages, including simple mathematical operation and ease of implementation. However, this model is of poor quality because it is highly dependent on the number of data used; fewer data points provide less accuracy [70].

$$CS, SL = \alpha_1(C)^{\alpha_2} * (w/b)^{\alpha_3} * (FA)^{\alpha_4} * (S)^{\alpha_5} * (CA)^{\alpha_6} * (SP)^{\alpha_7} \quad (3)$$

where the CS, SL, C, w/b, FA, S, CA, and SP are the compressive strength, slump flow diameter, cement (kg/m^3), water-to-binder ratio, fly ash (kg/m^3), sand (kg/m^3), coarse aggregate (kg/m^3), and superplasticizer (%), respectively. In addition, $\alpha_1, \alpha_2, \alpha_3, \alpha_4, \alpha_5, \alpha_6$, and α_7 are the model parameters.

2.4.3. Artificial Neural Network (ANN) Model

The ANN model [71–75] is a computer system of artificial neurons that function as fundamental units and mimic the parallel processes to analyze data like the human brain. The pattern of neuron connections influences the behavior of ANN networks, which also determines the network class. The ANN model can handle a mapping problem by estimating the relationship between input and output variables and distinguishing it from other expert systems by learning automatically from the obtained training patterns [76]. The ANN model is a machine learning system used in construction engineering for various numerical predictions and challenges [76–79]. The model is constructed based on three layers, input, hidden, and output, linked by biases and weights [80,81]. Several parameters affect the final model result, such as the number of hidden layers and neurons, the training algorithm, and the transfer function [82]. The ANN structure can be discovered by tuning the required parameters through trial and error.

The current study designed a multi-layer feed-forward network with SCC components (C, w/b, FA, S, CA, and SP) as input and the CS or SL as output. In the output layer, a sigmoid activation function was utilized. The typical process of the ANN result is shown in Figure 6. Equation (4) can be considered as a general formula for the calculation of an ANN output with only one node:

$$Output = bias + \sum_{j=1}^n (x_j \times w_j) \quad (4)$$

$$\beta_n = a_n(C) + b_n(w/b) + c_n(FA) + d_n(S) + e_n(CA) + f_n(SP) \quad (4a)$$

$$CS, SL = \frac{Node1}{1 + e^{-\beta_1}} + \frac{Node2}{1 + e^{-\beta_2}} + \dots + \frac{Node_n}{1 + e^{-\beta_n}} + Threshold \quad (4b)$$

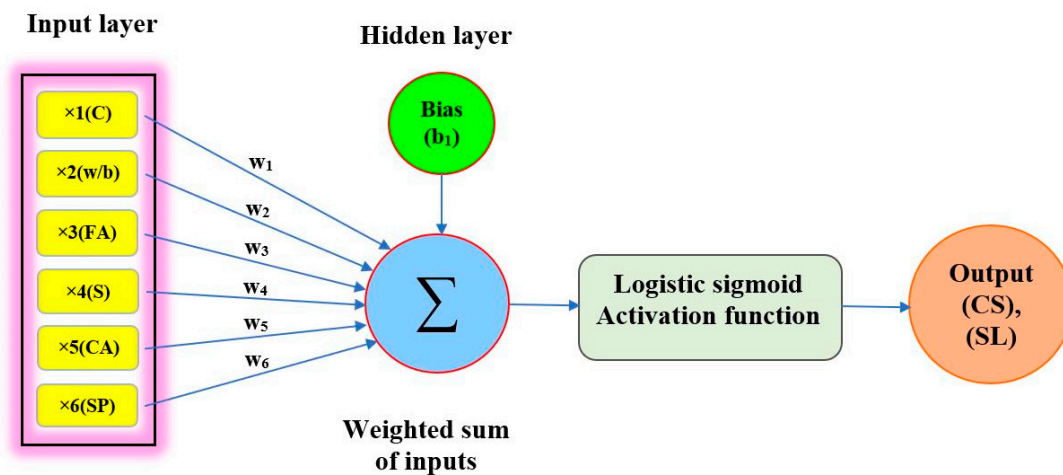


Figure 6. Typical ANN output procedure in a single node.

2.5. Metrics for Assessing Developed Models

The performance of the developed models was evaluated and characterized based on various assessment tools such as the Correlation Coefficient (R^2), Mean Absolute Error (MAE), Root Mean Squared Error (RMSE), Objective (OBJ), and Scatter Index (SI). The equations of these parameters are well defined in Table 3. R^2 is the squared correlation between the measured and predicted values. The greater the R-squared value, the more accurate the model. The average error made by models in predicting the outcome of the observation was measured by the RMSE. The OBJ function identified evaluation objectives based on the training and testing datasets and a variety of data.

Table 3. The performance evaluation criteria for the developed models.

Parameter	Equation	Range	Best Value
R^2 [58,80]	$R^2 = \left(\frac{\sum_i (vp - \bar{u}) \times (vi - \bar{v})}{\sqrt{\sum_i (vp - \bar{u})^2} \times \sqrt{\sum_i (vi - \bar{v})^2}} \right)^2$	0 – 1	1
MAE [24,80]	$MAE = \frac{\sum_{i=1}^n (vi - vp)}{n}$	0 – ∞	0
RMSE [24,69]	$RMSE = \sqrt{\frac{\sum_{i=1}^n (vi - vp)^2}{N}}$	0 – ∞	0
OBJ [58,80]	$OBJ = \left(\frac{n_{tr}}{n_{all}} \times \frac{MAE_{tr} + RMSE_{tr}}{R_{tr}^2 + 1} \right) + \left(\frac{n_{tst}}{n_{all}} \times \frac{MAE_{tst} + RMSE_{tst}}{R_{tst}^2 + 1} \right)$	0 – ∞	0
SI [69,80]	$SI = \frac{RMSE}{vi}$	<0.1	Excellent
		0.1 to 0.2	Good
		0.2 to 0.3	fair
		>0.3	Poor

Notes: vp = predicted value of compressive strength or slump flow; vi = experimental value of compressive strength or slump flow; \bar{u} = average of predicted compressive strength or slump flow; \bar{v} = average of experimental compressive strength or slump flow data; n = number of the dataset (training or testing); n_{tst} = number of the testing dataset; n_{tr} = number of the training dataset; n_{all} = total number of datasets (including training and testing).

3. Results and Discussion

3.1. Relation between Predicted and Experimental Values

3.1.1. Nonlinear Regression (NLR) Model

The Nonlinear Regression model was utilized to predict the compressive strength and slump flow diameter of FA-modified SCC. The NLR model results for CS and SL prediction are shown in Equations (5) and (6), respectively. The relationship between the measured

and predicted CS and SL values is displayed in Figure 7. When predicting the compressive strength, the training dataset was observed to have an R^2 of 0.81 and an RMSE value of 5.82 MPa. The testing dataset had an R^2 of 0.84 and RMSE of 7.67 MPa. In the testing dataset, the error line was from +50 to -25%, indicating that 25% of the data fell between 0.75 and 1.5 for the predicted to measured compressive strength ratio.

Regarding predicting the SL of FA-modified SCC, the training dataset had an R^2 of 0.82 and an RMSE of 11.6 mm. Also, the testing dataset had an R^2 of 0.57 and an RMSE of 27.4 mm. The error line was from +20 to -6% for the training data, indicating that 74% of the data fell between 0.94 and 1.2 for the predicted to experimental slump flow diameter ratio.

The NLR model provided nearly the same relationship value regarding R^2 based on the training dataset for both the CS and SL predictions.

$$CS = 14.1(C)^{0.32} + 1151.8(w/b)^{-0.03} + 0.42(FA)^{0.52} - 4.0(S)^{-14.45} - 5.1(CA)^{-13.96} - 1226(SP)^{0.00006} \quad (5)$$

No. of training dataset = 216, $R^2 = 0.81$, RMSE = 5.82 MPa

$$SL = 1242(C)^{-0.107} + 0.0001(w/b)^{0.0001} + 31.4(FA)^{0.026} - 0.0004(S)^{-0.0004} - 0.0002(CA)^{-0.0002} + 0.00001(SP)^{0.0002} \quad (6)$$

No. of training dataset = 60, $R^2 = 0.82$, RMSE = 11.6 mm

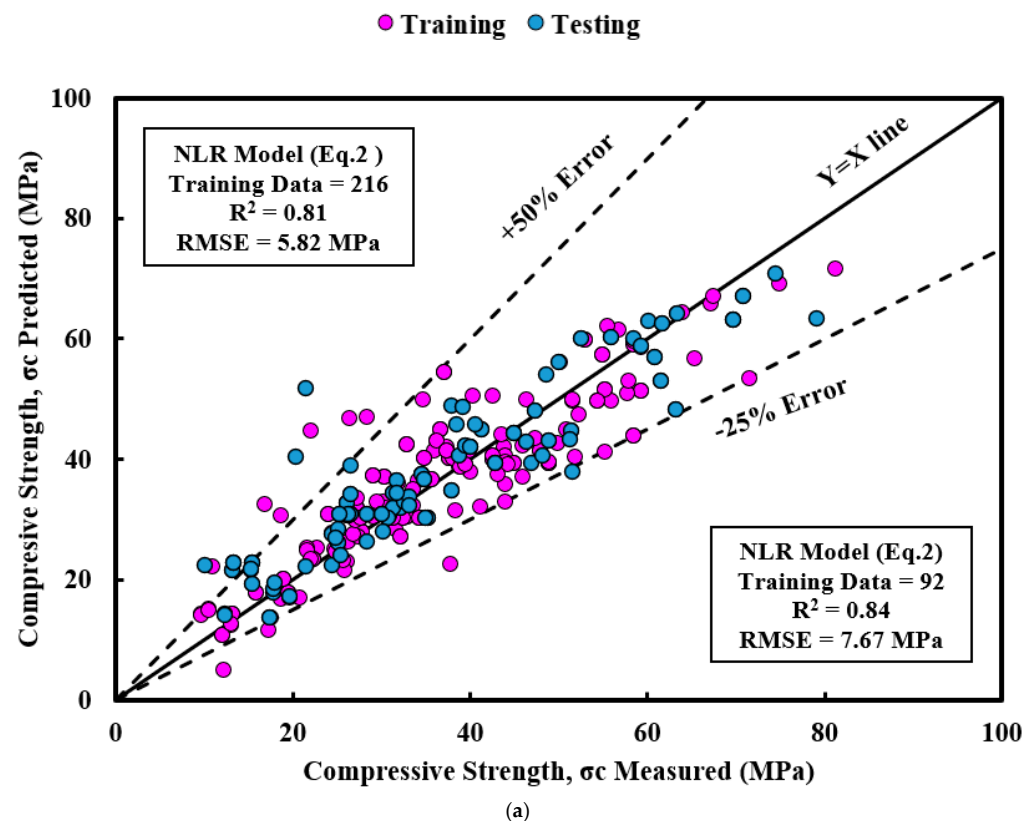


Figure 7. Cont.

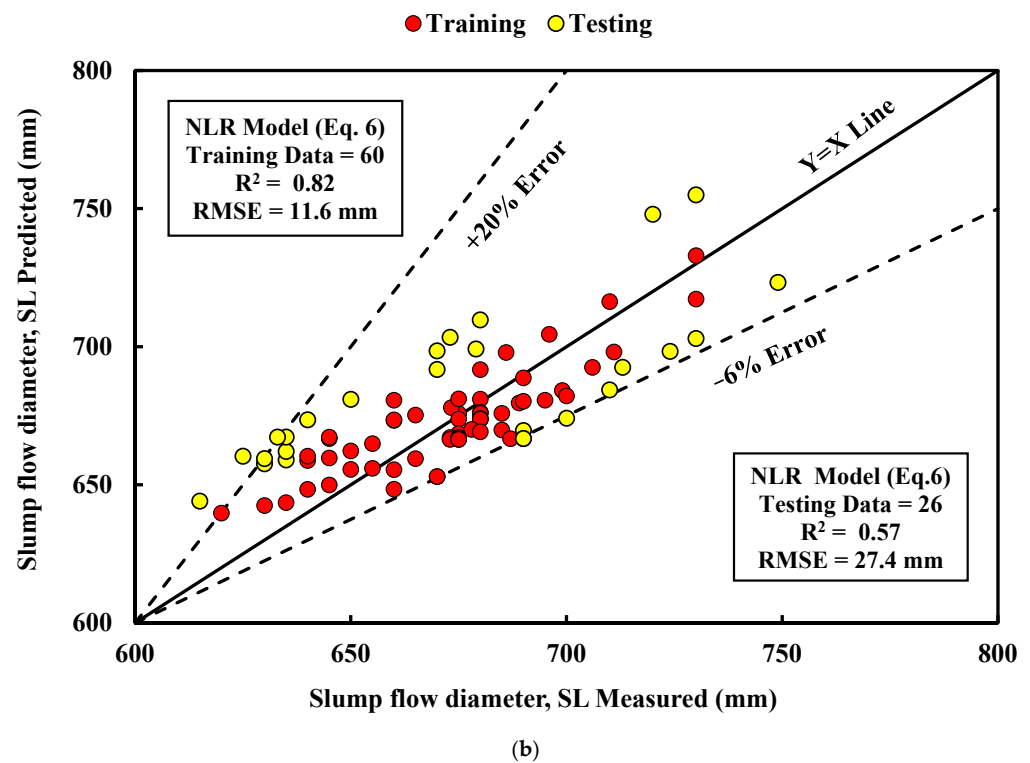


Figure 7. Comparison between the measured and predicted (a) CS and (b) SL using the NLR model for the training and testing datasets.

3.1.2. Multi-Linear Regression (MLR) Model

The Multi-Linear Regression model is another model used to predict the compressive strength and slump flow diameter of self-compacted concrete modified with fly ash. The MLR model has a simple mathematical expression. Therefore, it is considered one of the least effective models. The MLR model formula comprises constant terms and terms raised to the power of constant variables. In predicting compressive strength, the variables and their relationships are detailed in Equation (7). The relationship between variables in predicting the slump flow diameter is presented in Equation (8). The relationships between the predicted CS and SL with the experimental values are illustrated in Figure 8.

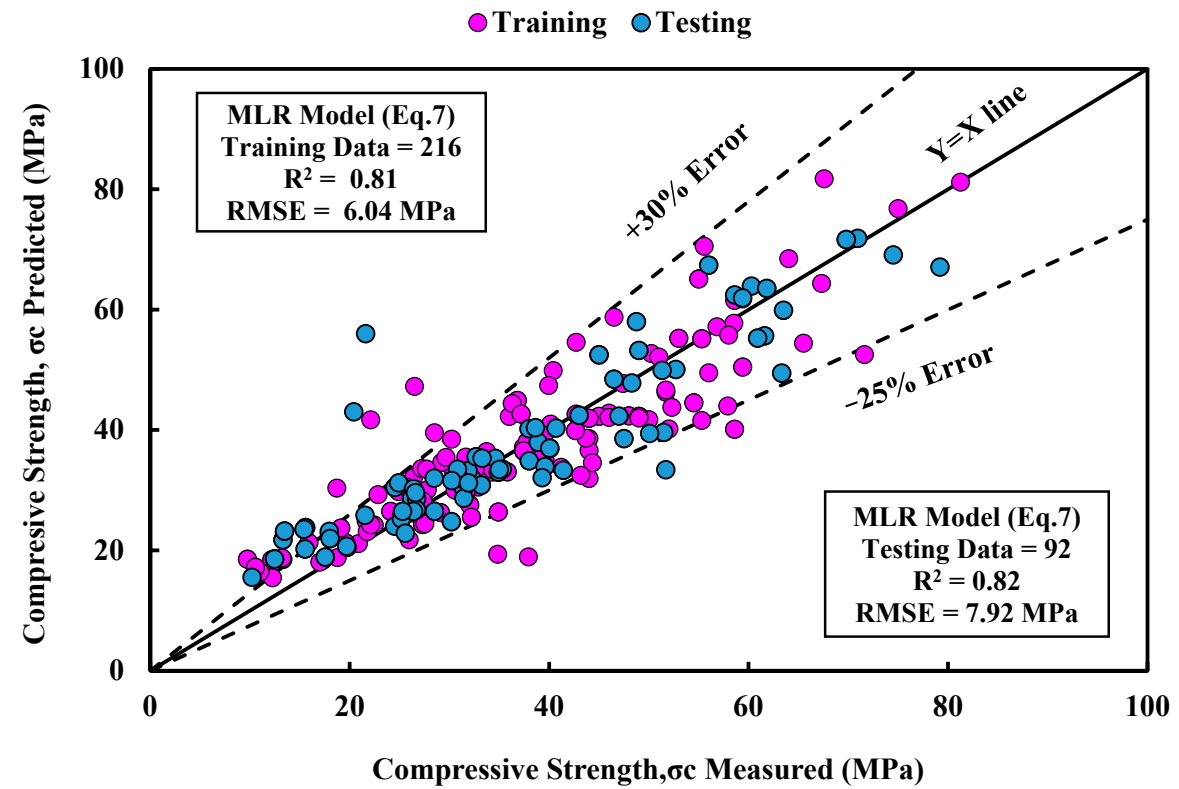
As displayed in Figure 8a, while predicting the CS of FA-modified SCC, the R^2 and RMSE were 0.81 and 6.04 MPa for training and 0.82 and 7.92 MPa for testing data, respectively. The error line was from +30 to −25% for training, meaning 45% of the data fell between 0.75 and 1.3 for the predicted to measured compressive strength ratio. Figure 8b presents the MLR model results when predicting the SL. The training dataset has an R^2 of 0.86 and an RMSE of 10.3 mm. However, the testing dataset has an R^2 of 0.57 and an RMSE of 26.8 mm. The error line ranges for training from +12 to −15%, implying that 73% of the data falls between 0.85 and 1.12 for the predicted to measured slump flow ratio.

$$CS = 0.0000003(C)^{0.8}(w/b)^{-0.88}(FA)^{0.015}(S)^{0.89}(CA)^{1.1}(SP)^{0.0063} \quad (7)$$

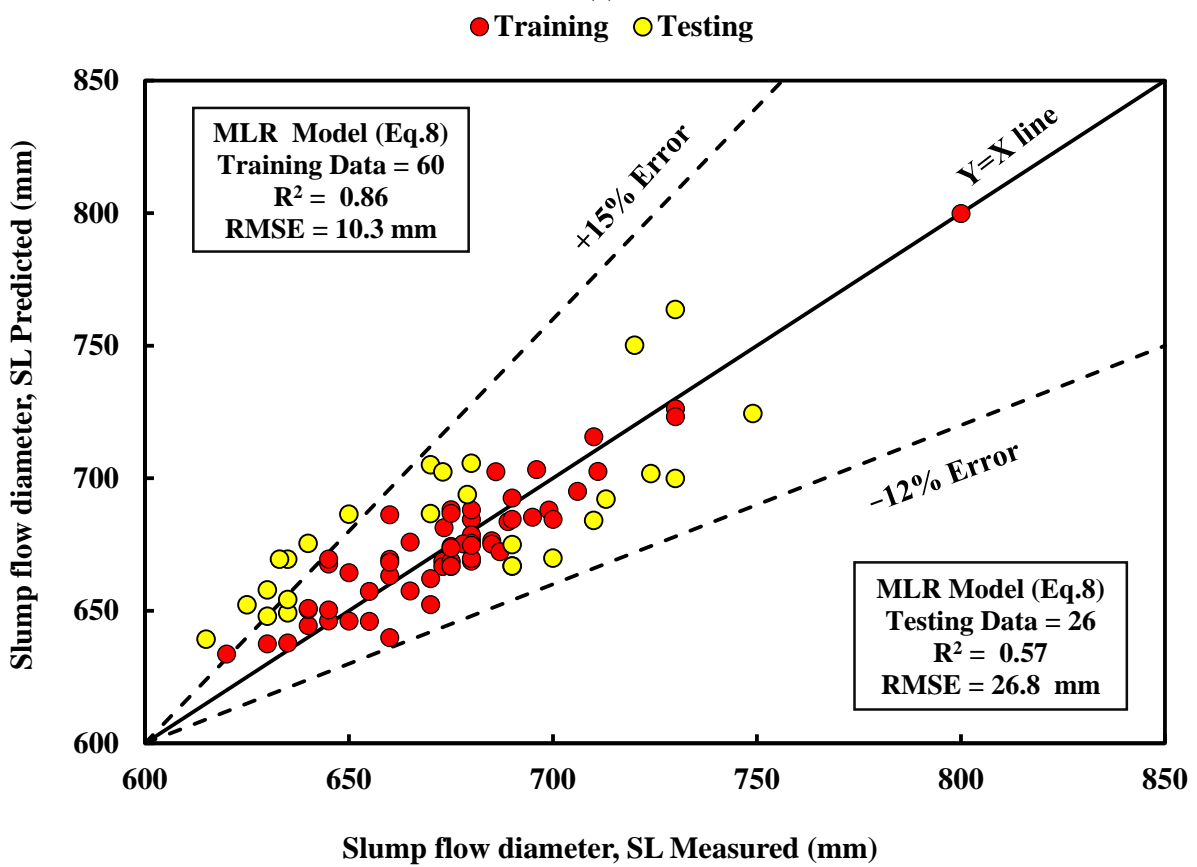
No. of training dataset = 216, $R^2 = 0.81$, RMSE = 6.04 MPa

$$SL = 1200(C)^{-0.09}(w/b)^{0.04}(FA)^{0.0009}(S)^{-0.0054}(CA)^{0.0086}(SP)^{-0.0028} \quad (8)$$

No. of training dataset = 60, $R^2 = 0.86$, RMSE = 10.3 mm.



(a)



(b)

Figure 8. Comparison between the measured and predicted (a) CS and (b) SL using thr MLR model for the training and testing datasets.

3.1.3. Artificial Neural Network (ANN) Model

An Artificial Neural Network was the last model used to predict the compressive strength and slump flow diameter of FA-modified SCC. The ANN network structure is known to be an excellent model for prediction. The ANN model was developed for various trials. As shown in Figure 9, the five trials (4, 6, 8, 10, and 12) were chosen based on their RMSE and MAE values for both the CS and SL training datasets independently. Then, the network with one hidden layer and six neurons had the lowest RMSE and MAE values in both predictions. Therefore, the ANN network having one hidden layer with six neurons with a Learning rate of 0.2, a Learning time of 2000, and 0.1 of momentum was selected (Figure 10).

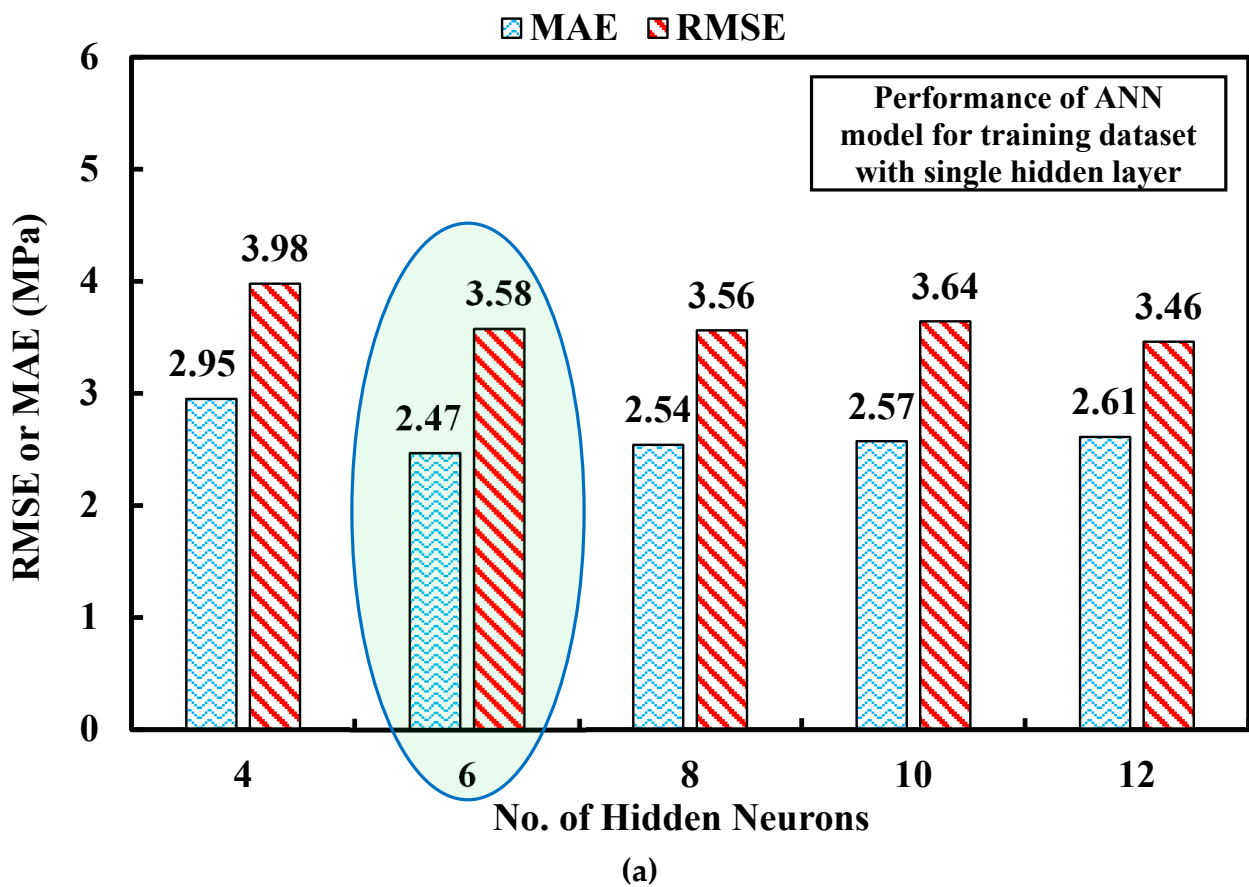


Figure 9. Cont.

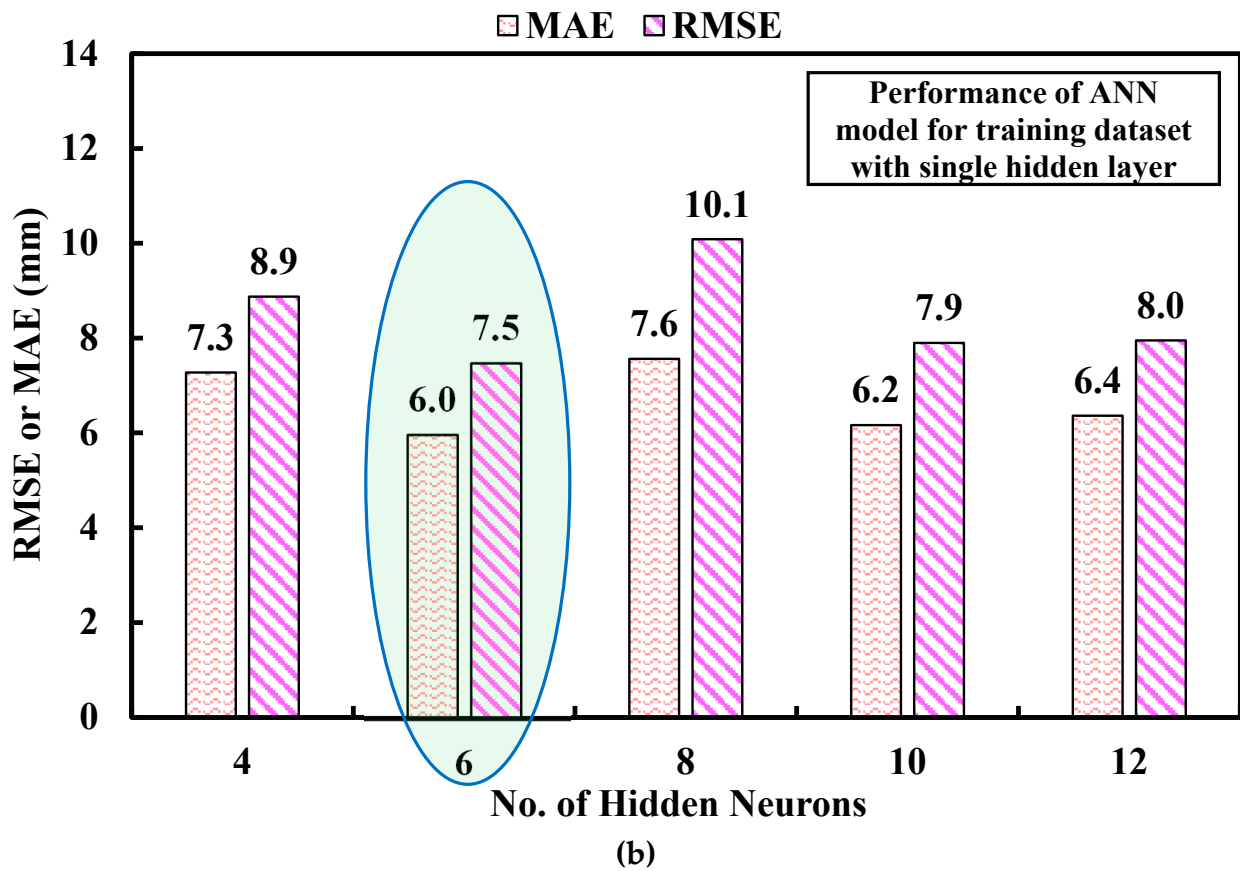


Figure 9. The RMSE and MAE values to select the optimum ANN. (a) CS and (b) SL.

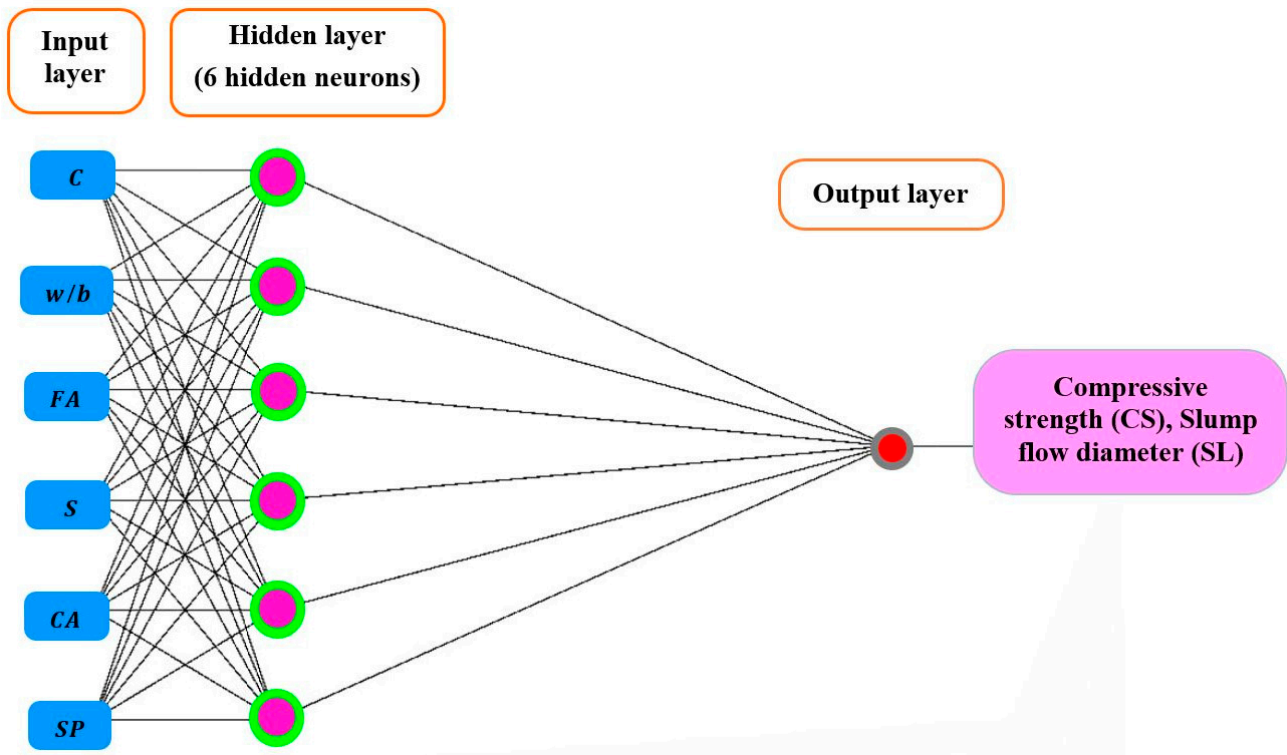


Figure 10. Optimal ANN network structures containing one hidden layer and six hidden neurons for predicting the CS and SL.

Equations (9) and (10) show the ANN formula for the CS and SL prediction, including weights and biases. Based on the training dataset, the ANN network analysis predicted a CS with an R^2 of 0.94 and an RMSE of 3.56 MPa. When the testing data were used, the model had an R^2 of 0.95 and an RMSE of 3.49 MPa. The training dataset had an error line from +20 to −20%, indicating that 80% of the data fell between 0.8 and 1.2 for the predicted to measured compressive strength ratio (Figure 11a). Concerning the SL prediction, the ANN network analysis predicted the SL with an R^2 of 0.93 and an RMSE of 7.5 mm when using the training data. However, when the tested data were used, the model had an R^2 of 0.997 and an RMSE of 2.2 mm. The error line for the training dataset was from +6 to −6%, indicating that 94% of the data fell between 0.94 and 1.06 for the predicted to measured SL ratio (Figure 11b).

$$\begin{bmatrix} 3.359 & 2.124 & 2.148 & 3.227 & -3.055 & -1.632 & -0.721 \\ -1.44 & -0.375 & 1.352 & 0.85 & -4.672 & 0.748 & -1.398 \\ -2.898 & 2.86 & -3.685 & -1.624 & -1.919 & -1.0 & -1.278 \\ 1.676 & 2.417 & -0.28 & 0.863 & -2.15 & -0.516 & -2.244 \\ 0.566 & 0.664 & 2.387 & -0.666 & 2.182 & -0.175 & -1.704 \\ -5.371 & 0.485 & -0.725 & -4.055 & 1.378 & -0.933 & -5.319 \end{bmatrix} \times \begin{bmatrix} c \\ w/b \\ FA \\ S \\ CA \\ SP \\ 1 \end{bmatrix} = \begin{bmatrix} \beta_1 \\ \beta_2 \\ \beta_3 \\ \beta_4 \\ \beta_5 \\ \beta_6 \end{bmatrix}$$

$$CS = \frac{1.567}{1 + e^{-\beta_1}} - \frac{0.795}{1 + e^{-\beta_2}} - \frac{0.848}{1 + e^{-\beta_3}} - \frac{1.771}{1 + e^{-\beta_4}} + \frac{1.392}{1 + e^{-\beta_5}} - \frac{0.681}{1 + e^{-\beta_6}} + 0.406 \quad (9)$$

No. of training dataset = 216, $R^2 = 0.94$, RMSE = 3.65 MPa.

$$\begin{bmatrix} -0.727 & -1.185 & -0.596 & 0.933 & -1.821 & -0.152 & -0.964 \\ 0.994 & 2.508 & 0.733 & 0.542 & 1.019 & 0.152 & -1.545 \\ 2.787 & -2.651 & -2.147 & -2.421 & 0.832 & -1.129 & -0.083 \\ -0.933 & -0.718 & 0.339 & 1.166 & 3.153 & 2.376 & -1.338 \\ 0.506 & 0.705 & 1.46 & 0.25 & -0.421 & -0.534 & -1.808 \\ -1.071 & 0.003 & 1.204 & -0.509 & -0.073 & 0.813 & -1.665 \end{bmatrix} \times \begin{bmatrix} c \\ w/b \\ FA \\ S \\ CA \\ SP \\ 1 \end{bmatrix} = \begin{bmatrix} \beta_1 \\ \beta_2 \\ \beta_3 \\ \beta_4 \\ \beta_5 \\ \beta_6 \end{bmatrix}$$

$$SL = -\frac{1.508}{1 + e^{-\beta_1}} - \frac{1.372}{1 + e^{-\beta_2}} - \frac{1.025}{1 + e^{-\beta_3}} - \frac{1.441}{1 + e^{-\beta_4}} - \frac{1.326}{1 + e^{-\beta_5}} + \frac{0.933}{1 + e^{-\beta_6}} + 1.714 \quad (10)$$

No. of training dataset = 60, $R^2 = 0.93$, RMSE = 7.5 mm.

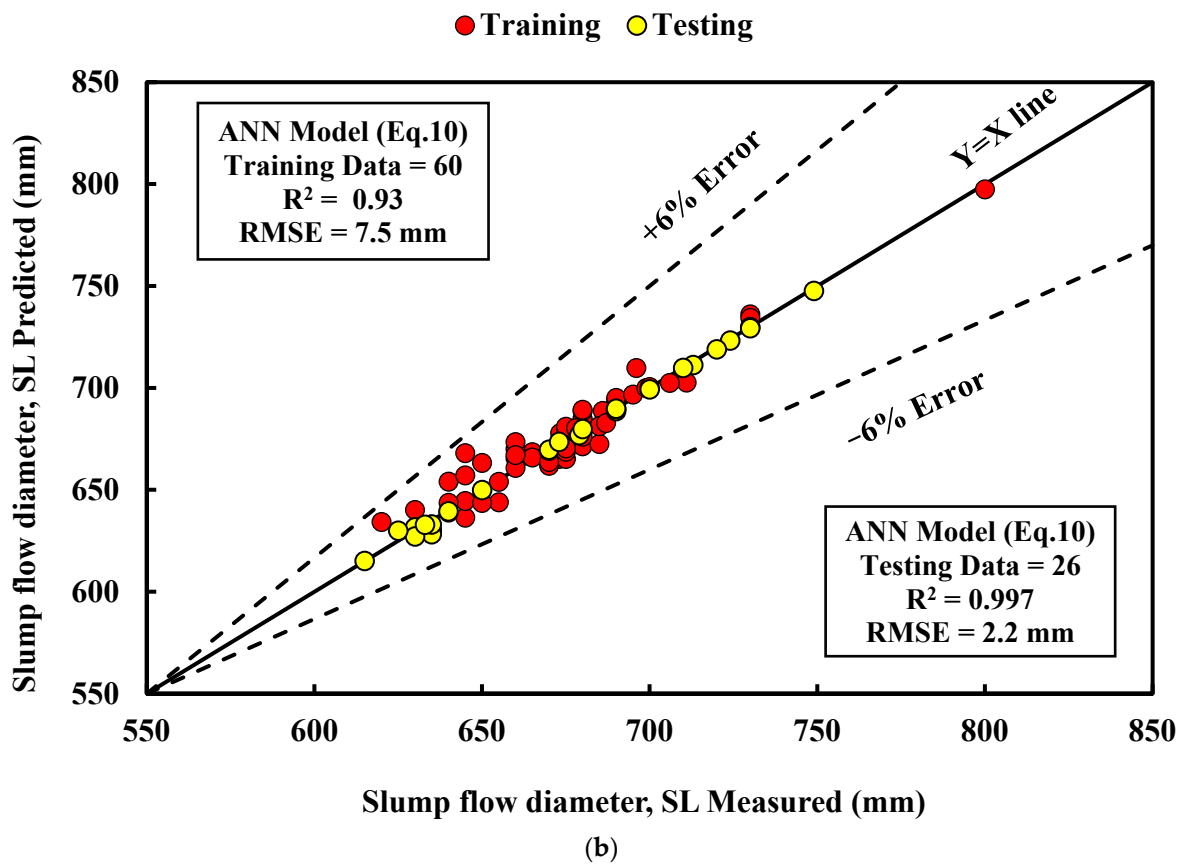
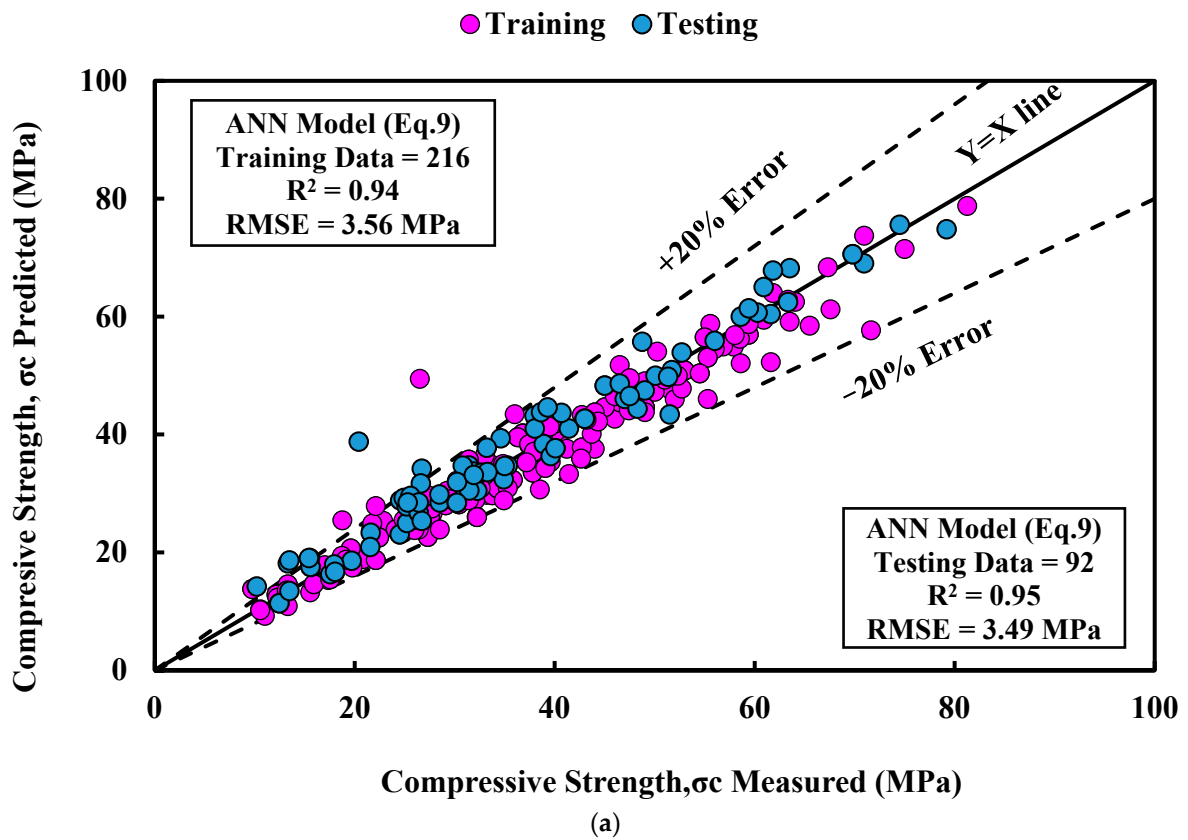


Figure 11. Comparison between the measured and predicted (a) CS and (b) SL using the ANN model for the training and testing dataset.

Since the measured compressive strength values in the training dataset were divided into three stages—LSC (less than 20 MPa), NSC (20 to 50 MPa), and HSC (greater than 50 MPa)—the ANN model was applied to all three stages, and the resulting R^2 , RMSE, and MAE values were all reported. The samples were 29, 143, and 44 for LSC, NSC, and HSC, respectively. The ANN model for LSC had an R^2 of 0.76, RMSE of 1.84 MPa, and MAE of 1.34 MPa. The model result differed for the middle stage (NSC); the R^2 was 0.77, the RMSE was 3.77 MPa, and the MAE had a value of 2.624 MPa. The HSC maintained greater result values, with an R^2 of 0.79, RMSE of 4.13 MPa, and MAE of 2.98 MPa (Figure 12).

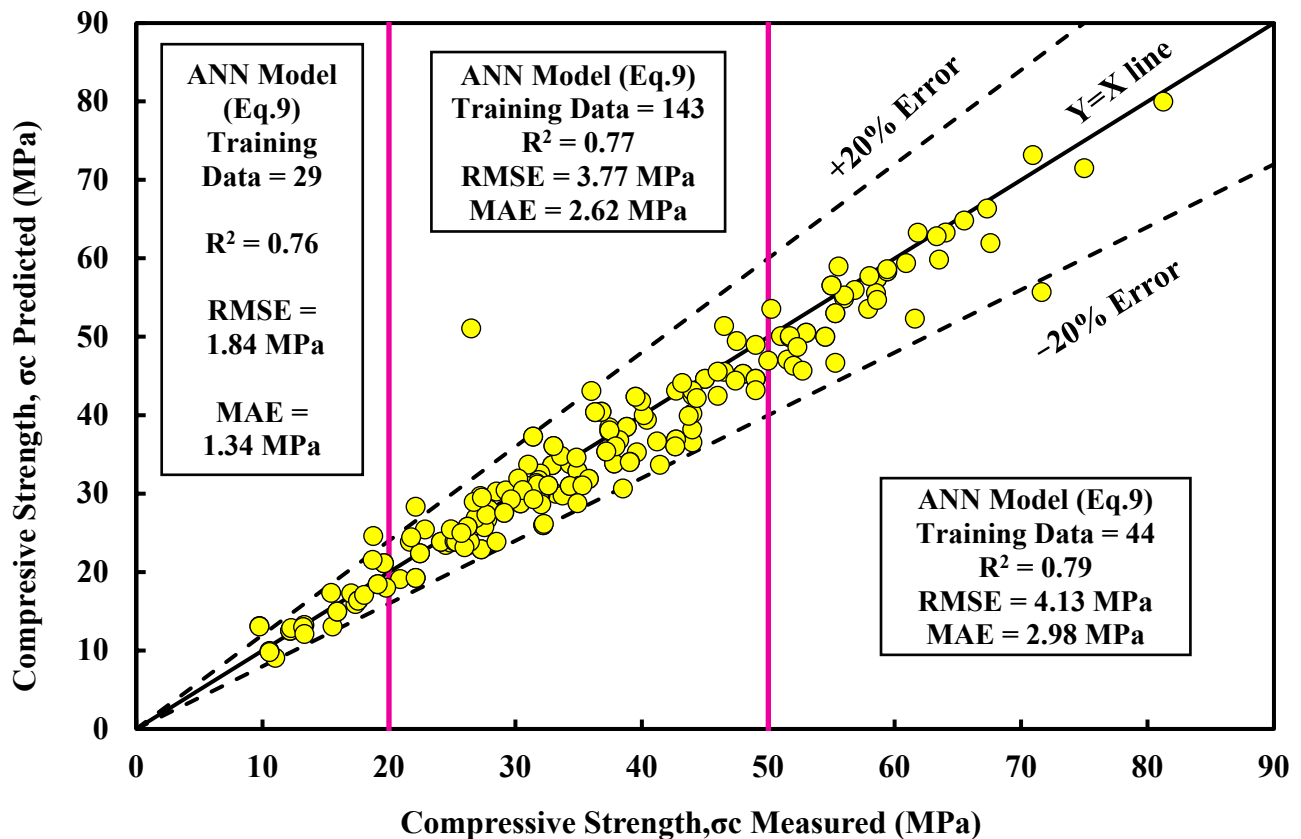


Figure 12. Relationship between the measured and predicted CS of FA-modified SCC for different ranges.

Furthermore, based on the training dataset, the slump flow diameter values were divided into classes 1, 2, and 3. The number of samples was 12 in the first class, 47 in the second class, and only 1 in the last. Due to the high sample number of class 2, the ANN model was applied to the class. The model provided an R^2 of 0.88, RMSE of 6.2 mm, and MAE of 5.2 mm (Figure 13).

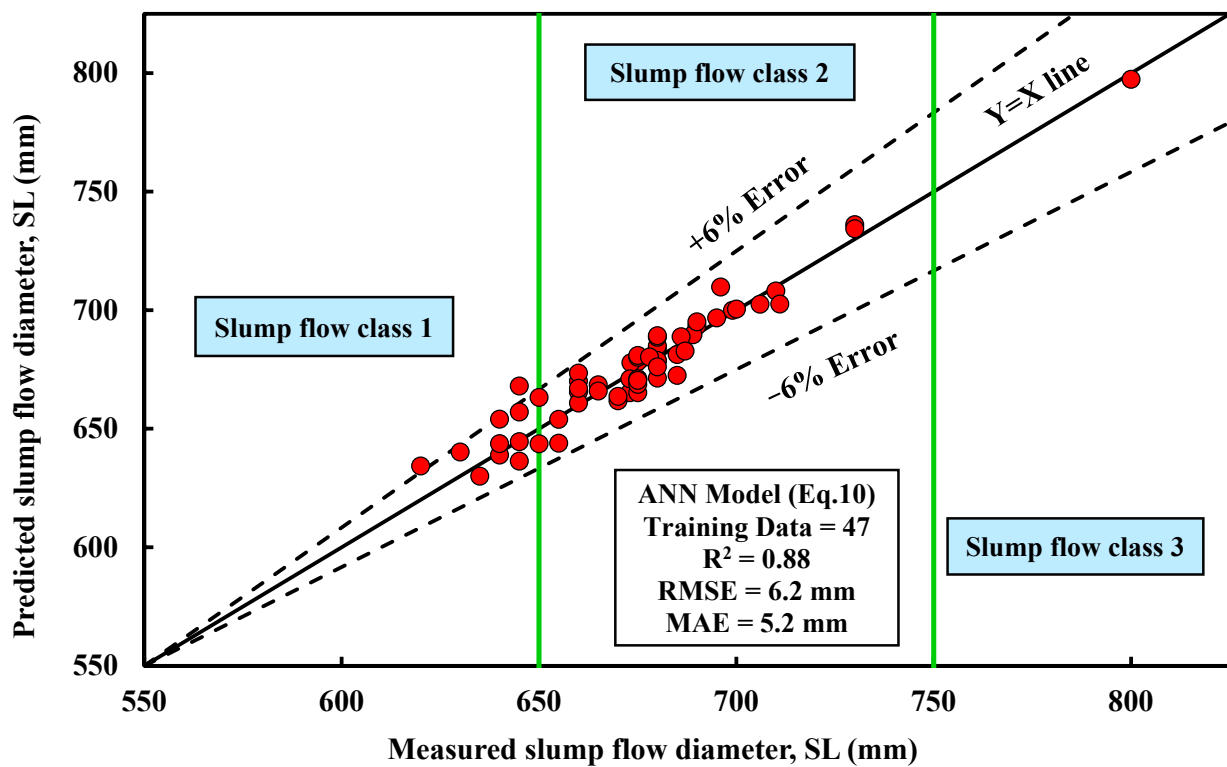
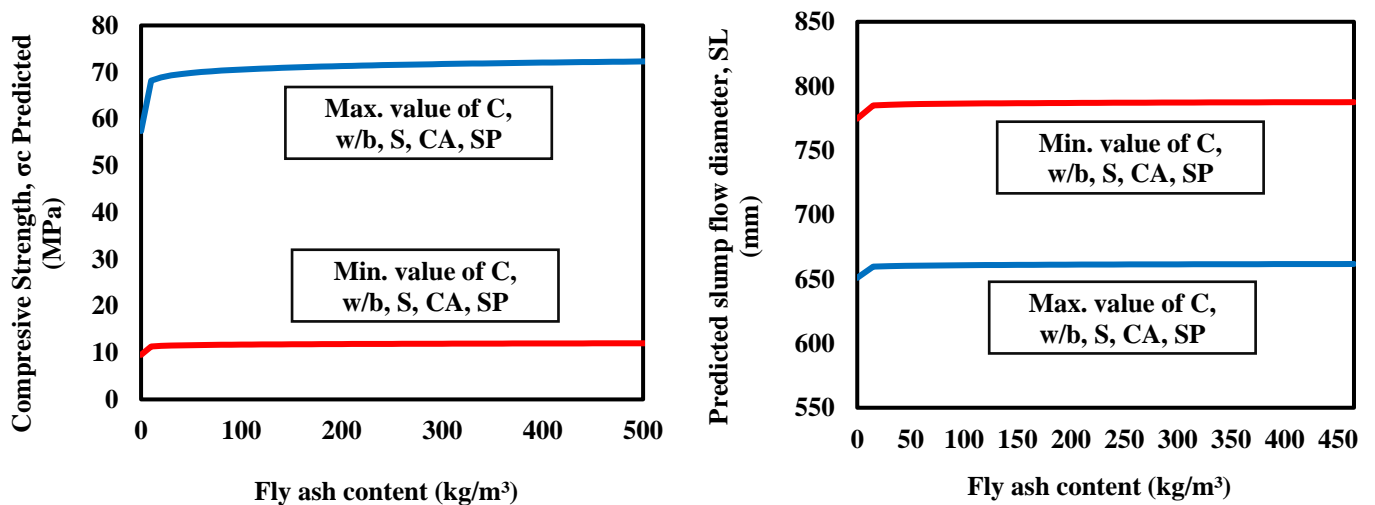


Figure 13. Relationship between the measured and predicted SL of FA-modified SCC for different classes.

3.2. Effective Factors

The effect of independent parameters such as cement, water-to-binder ratio, fly ash, sand, coarse aggregate, and superplasticizer on the compressive strength and slump flow diameter of self-compacted concrete was evaluated using the MLR model. The effect of a single parameter was found by changing its value from the minimum to the maximum by fixing other parameters on either the minimum value or the maximum value. The predicted CS and SL results were recorded in both cases, fixing independent variables at the minimum and the maximum. Figure 14 shows all the effects of both the CS and SL predictions.



(a)

Figure 14. Cont.

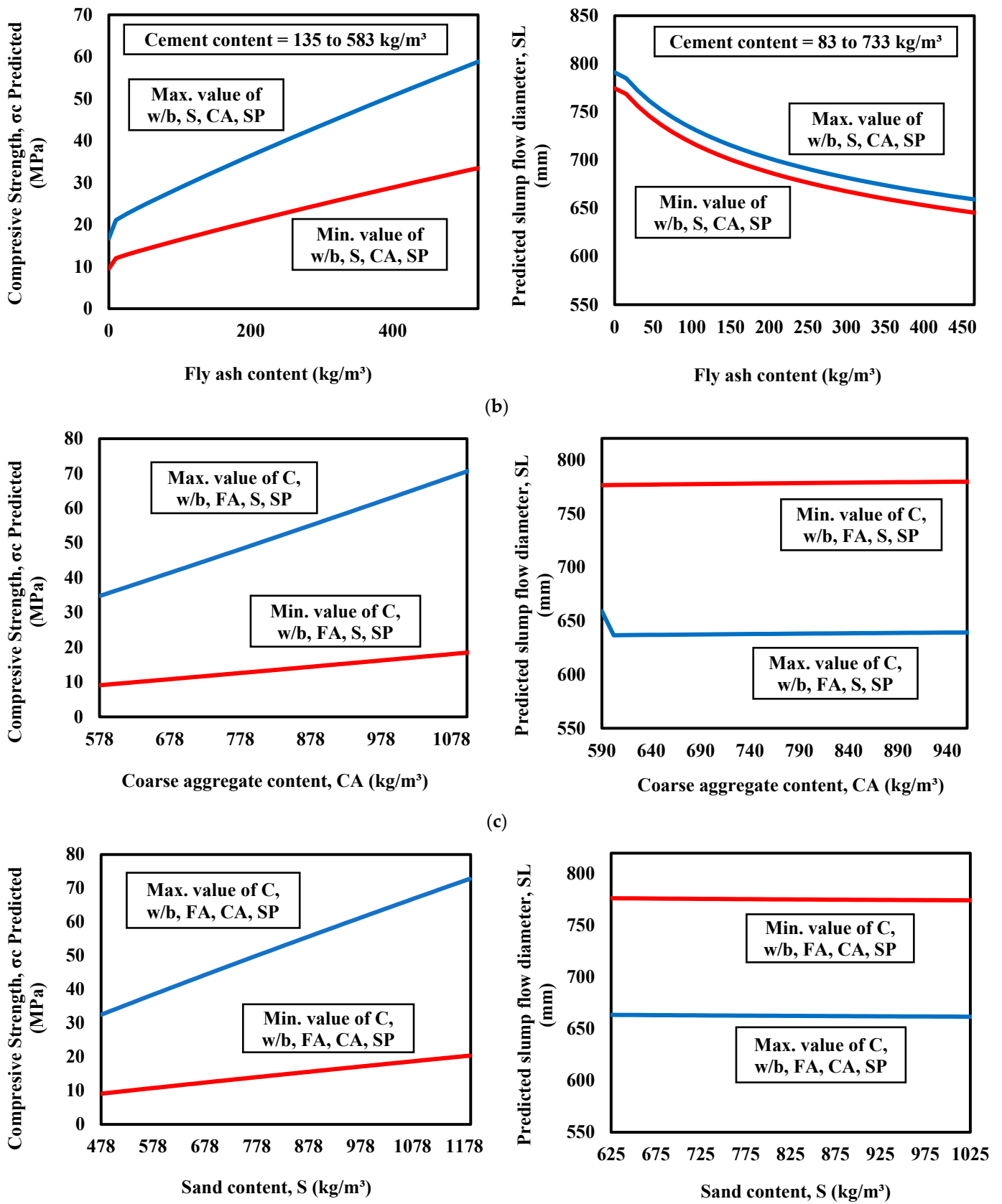


Figure 14. Cont.

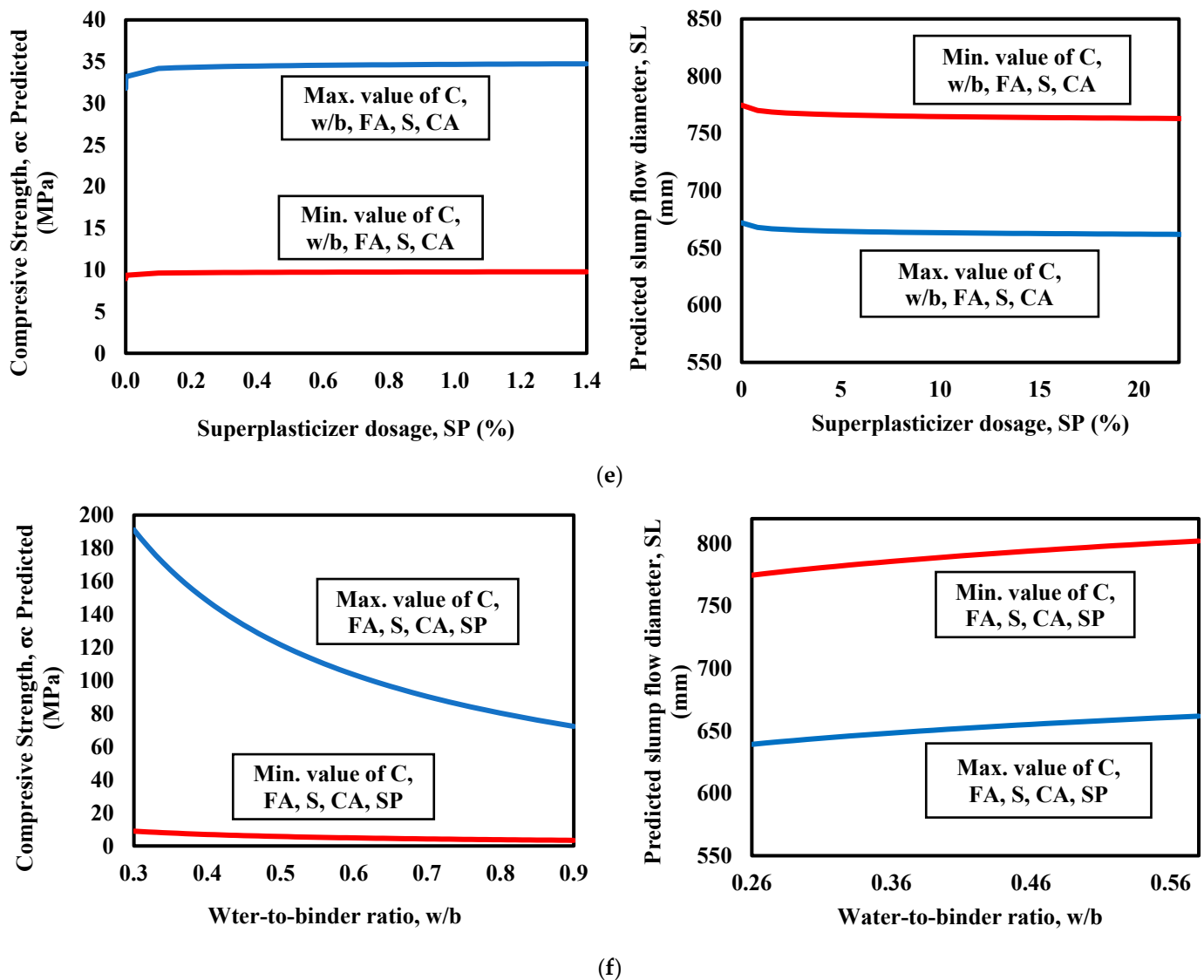


Figure 14. Effect of (a) fly ash content, (b) fly ash with cement content, (c) coarse aggregate content, (d) sand content, (e) superplasticizer dosage, and (f) water-to-binder ratio on the CS and SL of SCC.

The MLR model result noted that increasing the fly ash content caused an increased CS but had very little effect on the SL of SCC. Meanwhile, increasing the cement and fly ash content at the same time decreased the SL but increased the CS. The coarse aggregate and sand content greatly affected the CS. Increasing the CA and S content increased the CS. However, the effect of aggregates was less on the SL. Increasing the CA content increased the SL but decreased with the S content. On the other hand, superplasticizer was observed to have a small effect on the CS and SL.

From the CS prediction, it was noted that all the independent variables in their maximum value provided a greater value of CS when the value of any single parameter was changed. In contrast to CS, the greater value of SL was achieved while applying the minimum value of the independent variables. The summary of the most affected factors for both CS and SL is shown in Figure 15.

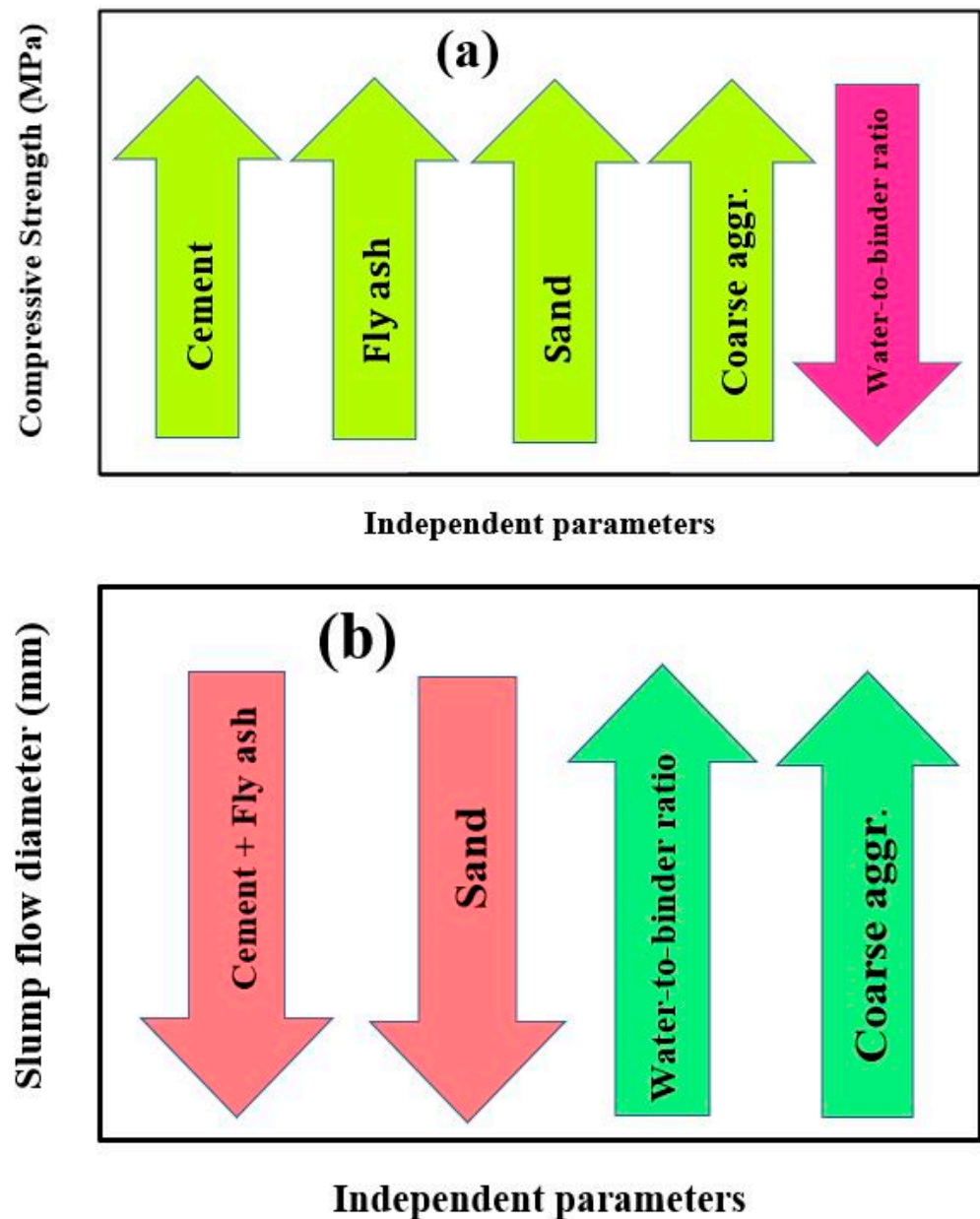


Figure 15. Effect of independent parameters on the (a) CS and (b) SL of SCC.

4. Evaluation of Developed Models

The study was conducted to determine the effect of different fly ash content on the compressive strength and slump flow diameter of self-compacted concrete. The experiment included predicting the CS and SL using three alternative models; NLR, MLR, and ANN. Each model provided a formula based on several mathematical parameters, and various assessment criteria were used to assess the performance of each constructed model.

Based on the R^2 , RMSE, and MAE values, the ANN model provided the highest accuracy and reliability for predicting compressive strength and slump flow diameter using the training dataset. For the CS prediction, the ANN model had an R^2 of 0.94, RMSE of 3.56 MPa, and MAE of 2.54 MPa based on the training dataset, as well as an R^2 of 0.95, RMSE of 3.49 MPa, and MAE of 2.45 MPa for the testing dataset. In terms of the SL prediction, the ANN model had an R^2 of 0.93, RMSE of 7.5 mm, and MAE of 5.97 mm based on the training dataset, and an R^2 of 0.997, RMSE of 2.2 mm, and MAE of 1.39 mm based on the testing dataset. All statistical results for all models are summarized in Table 4. Considering the error lines, the ANN was noted to have more data along the $Y=X$ line. For

CS, the model had an error line from +20 to −20% for the training dataset, indicating that 80% of the data were between 0.8 and 1.2 (predicted CS/experimental CS). However, in predicting the SL, the ANN model had an error line from +6 to −6% for the training dataset, indicating that 94% of the data were between 0.94 and 1.06 (predicted SL/experimental SL).

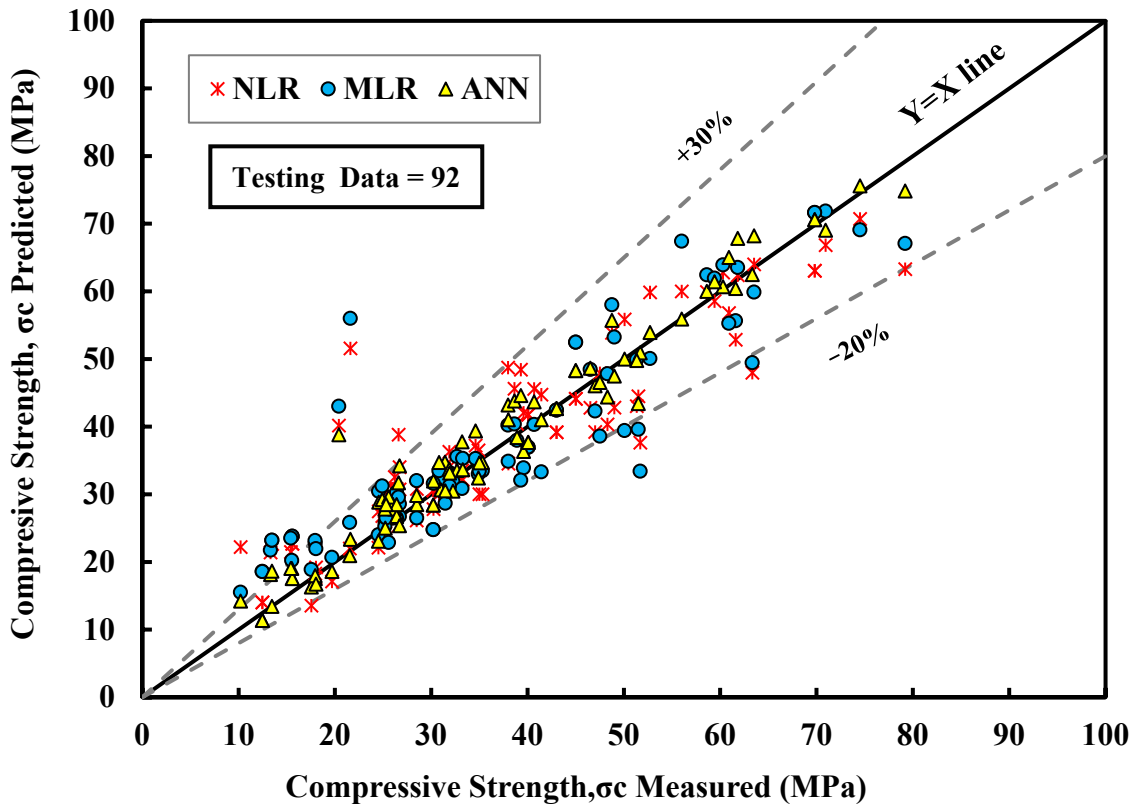
Table 4. Summary of the evaluation assessment criteria for the developed models in FA-modified SCC for the CS prediction.

Compressive strength	Model	Figure (No)	Equation (No.)	Training			Testing			Ranking
				R ²	RMSE (MPa)	MAE (MPa)	R ²	RMSE (MPa)	MAE (MPa)	
	NLR	7a	5	0.81	5.82	4.67	0.84	7.67	4.72	2
	MLR	8a	7	0.81	6.04	4.69	0.82	7.92	4.65	3
	ANN	11a	9	0.94	3.56	2.54	0.95	3.49	2.45	1
Slump flow diameter	Model	Figure (No)	Equation (No.)	Training			Testing			Ranking
				R ²	RMSE (mm)	MAE (mm)	R ²	RMSE (mm)	MAE (mm)	
	NLR	7b	6	0.82	11.6	10.12	0.57	27.4	27.1	3
	MLR	8b	8	0.86	10.3	8.54	0.57	26.8	25.93	2
	ANN	11b	10	0.93	7.5	5.97	0.997	2.2	1.39	1

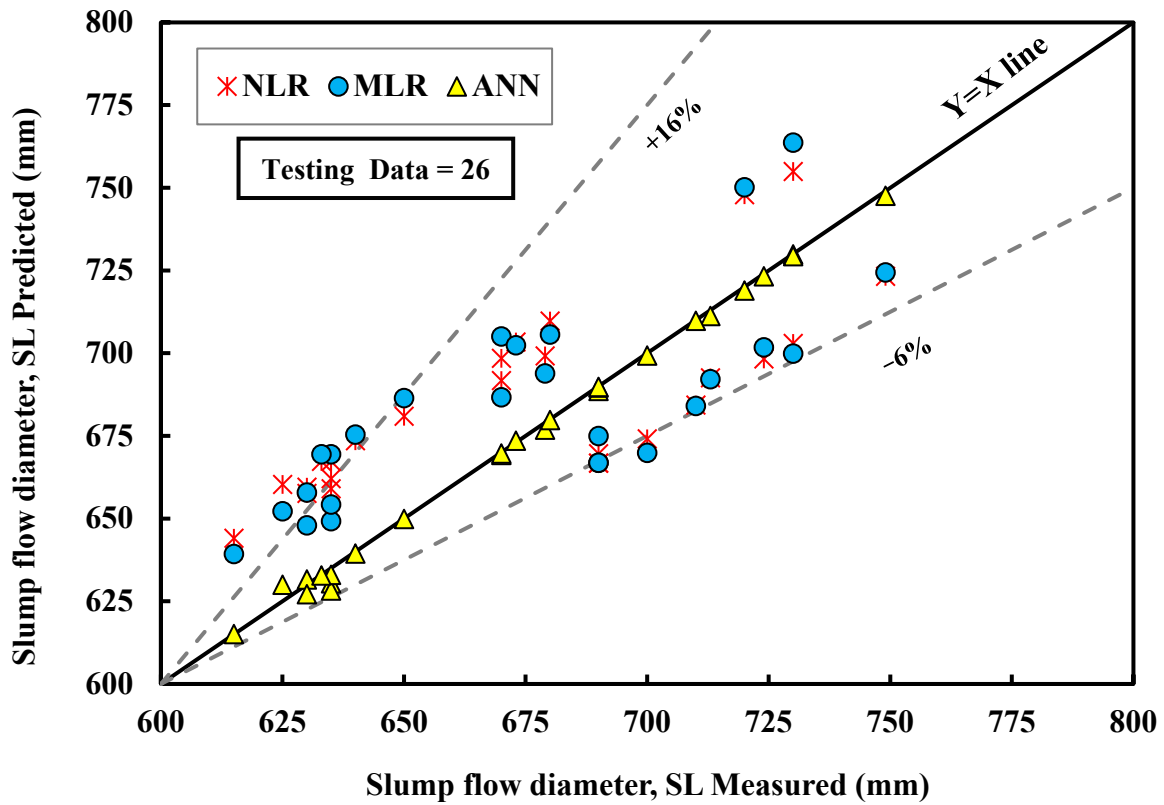
Furthermore, the second-ranked model was the NLR for CS prediction; it had an R² of 0.81, RMSE of 5.82 MPa, and MAE of 4.67 MPa for the training dataset, and R² of 0.84, RMSE of 7.67 MPa, and MAE of 4.72 MPa for the testing dataset. The model ranged between the +30 and −25% error lines for the training dataset. However, the MLR was second-ranked for the SL prediction; it had an R² of 0.86, RMSE of 10.3 mm, and MAE of 8.54 mm for the training dataset, and an R² of 0.57, RMSE of 26.8 mm, and MAE of 25.93 mm for the testing dataset. The error line was between +12 and −15% for the MLR model based on the training dataset.

Moreover, the training dataset from the collected data for CS prediction was divided into three different ranges, and then the ANN model was applied. All the R², RMSE, and MAE values were calculated. The ANN model for the low CS strength range had an R² of 0.76, RMSE of 1.84 MPa, and MAE of 1.34 MPa. The model result differed for the middle stage; the R² was 0.77, the RMSE was 3.77 MPa, and the MAE was 2.62 MPa. The high CS strength range maintained higher results, with an R² of 0.79, RMSE of 4.13 MPa, and MAE of 2.98 MPa. On the other hand, the training dataset for predicting the SL was divided into three classes, and the ANN model was used to calculate each class's R², RMSE, and MAE values. The model had an R² of 0.88, an RMSE of 6.2 mm, and an MAE of 5.2 mm for the mid-class (from 650 to 750 mm).

The testing dataset had lower R², RMSE, and MAE values than the training dataset for all the developed models predicting CS and SL. The variations to the measured values were plotted as shown in Figure 16 for the compressive strength and slump flow diameter of self-compacted concrete. Model values fell between the +30 and −20% error lines for CS prediction, and between −20% and +30% for the SL prediction, indicating poor performance.



(a)



(b)

Figure 16. Relationship between the measured and predicted (a) CS and (b) SL for the developed models using the testing dataset.

The performance of the developed models was also evaluated using the training and testing datasets through the OBJ function and SI value. According to the objective function, the ANN model maintained the lowest value using the training dataset (Figure 17). The OBJ value was 3.12 and 5.5 for the CS and SL, respectively. Based on the SI value, the NLR model showed an excellent performance in predicting the CS. The SI value was 0.10 for both the training and testing datasets. In predicting the SL, the NLR, MLR, and ANN models showed excellent performances for both the training and testing datasets. The SI value was 0.02 for both the NLR and MLR models and 0.01 for the ANN model (Figure 18).

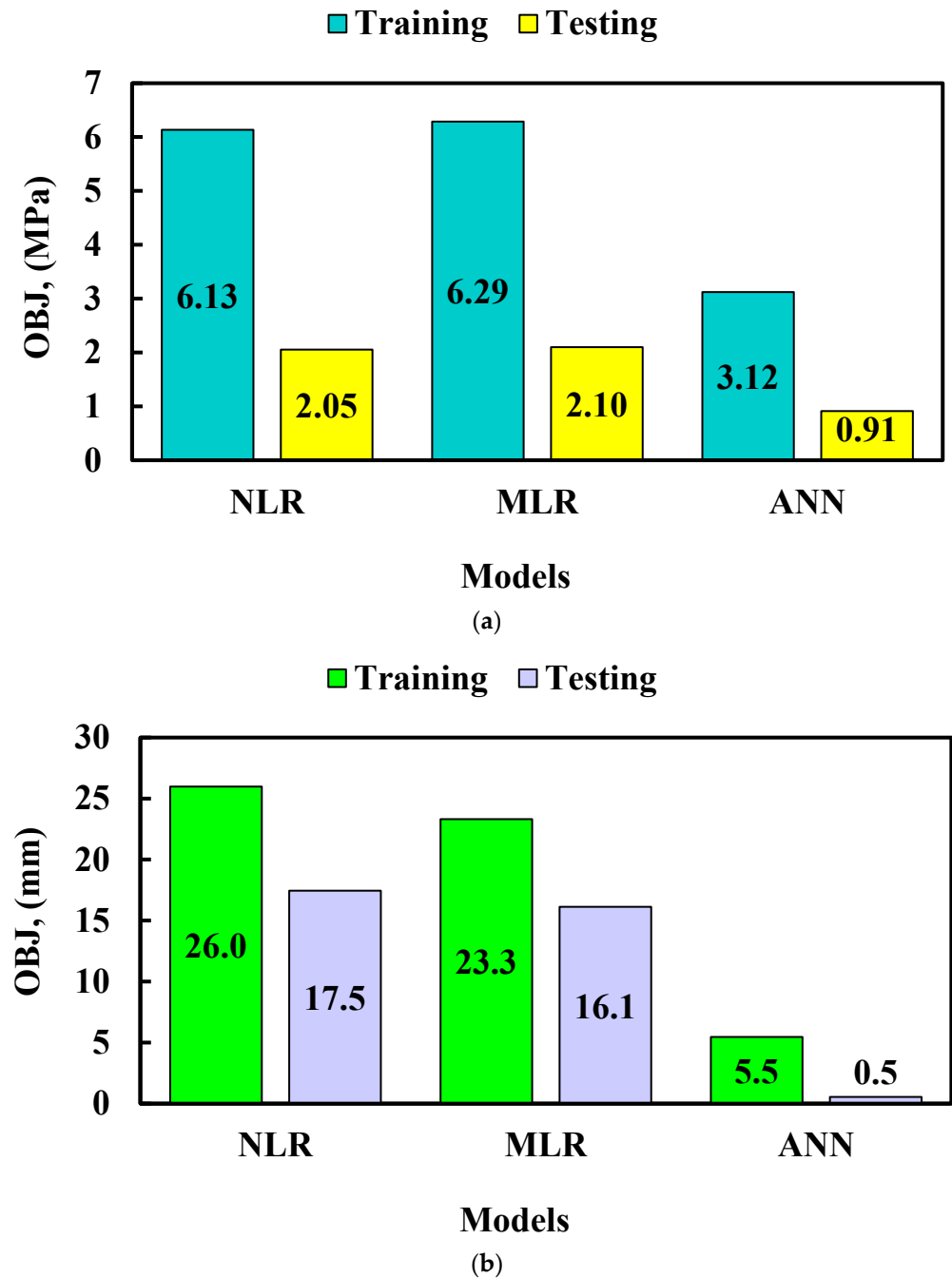
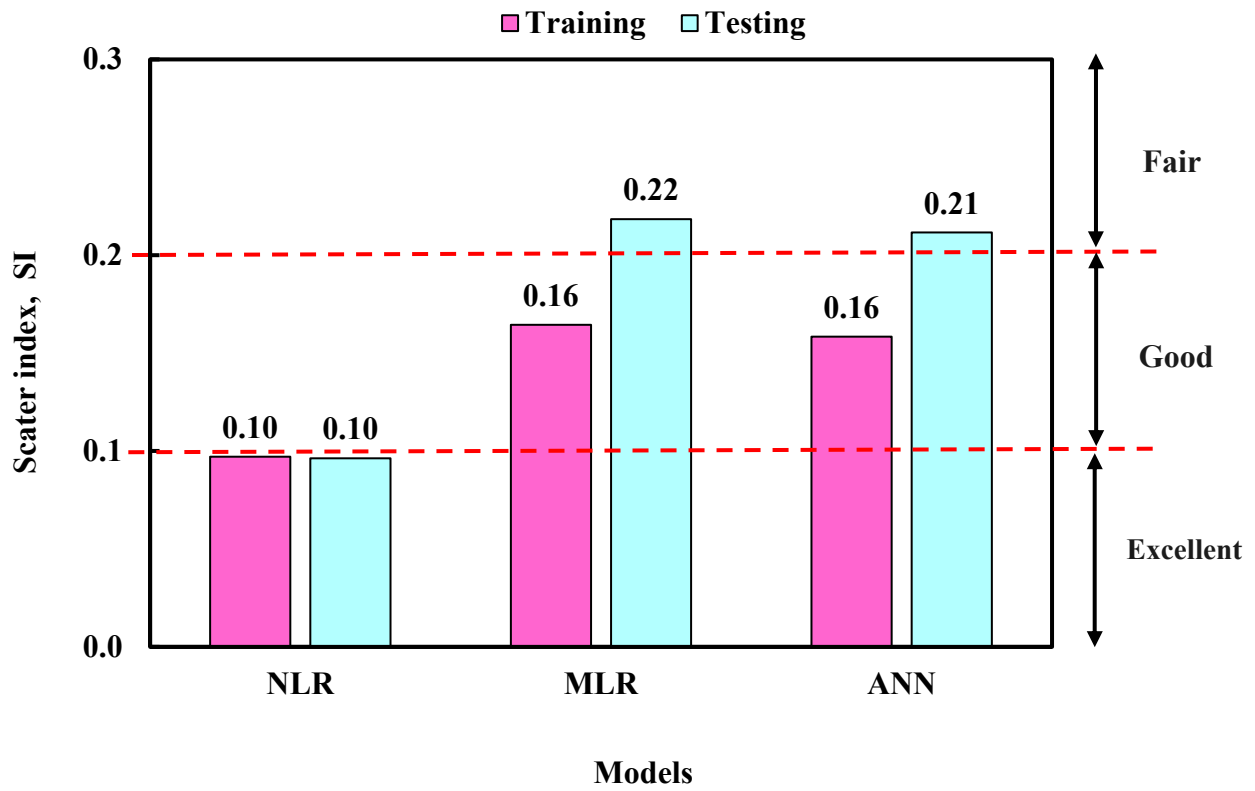
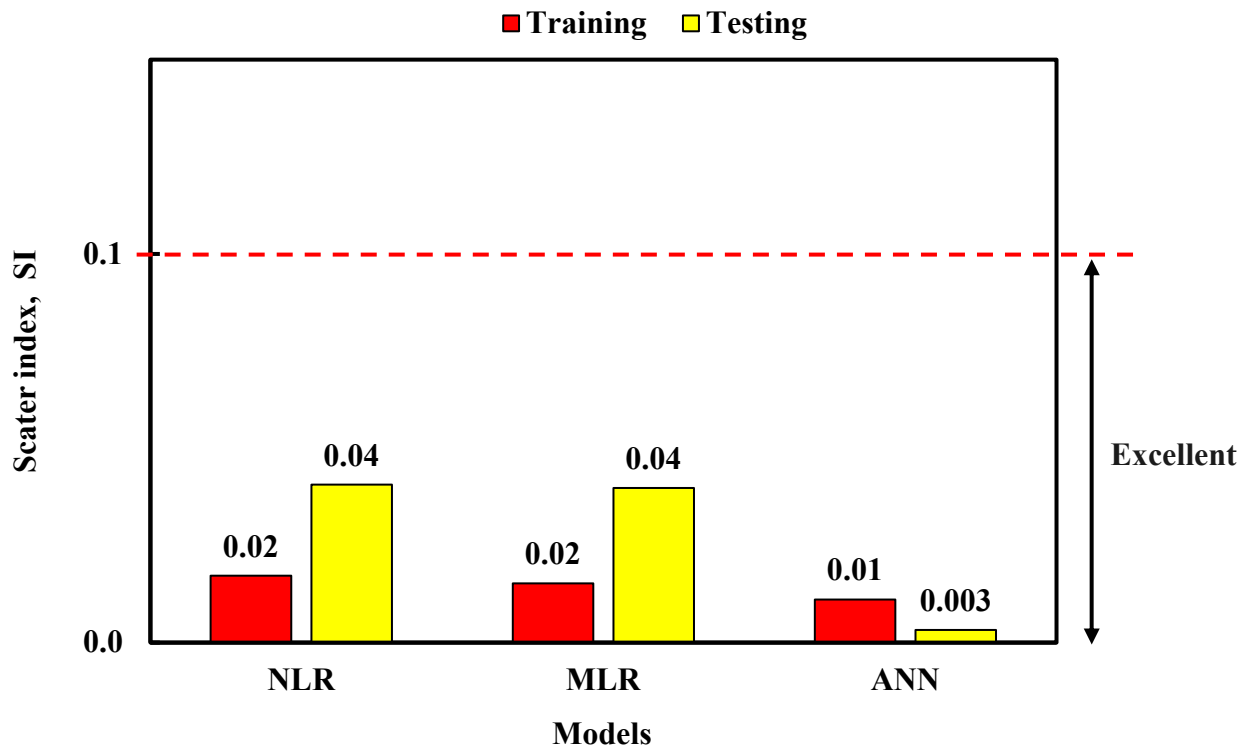


Figure 17. Comparison of the developed models using OBJ: (a) CS and (b) SL.



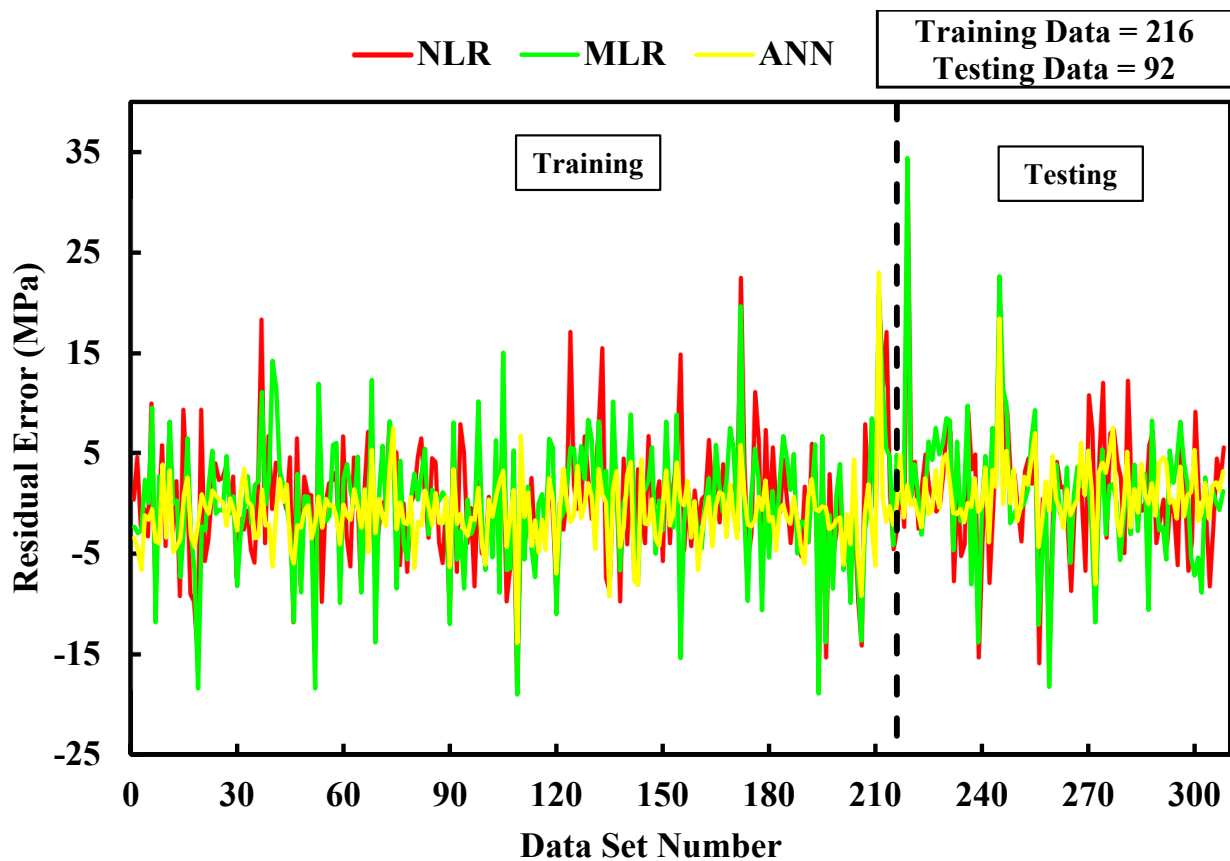
(a)



(b)

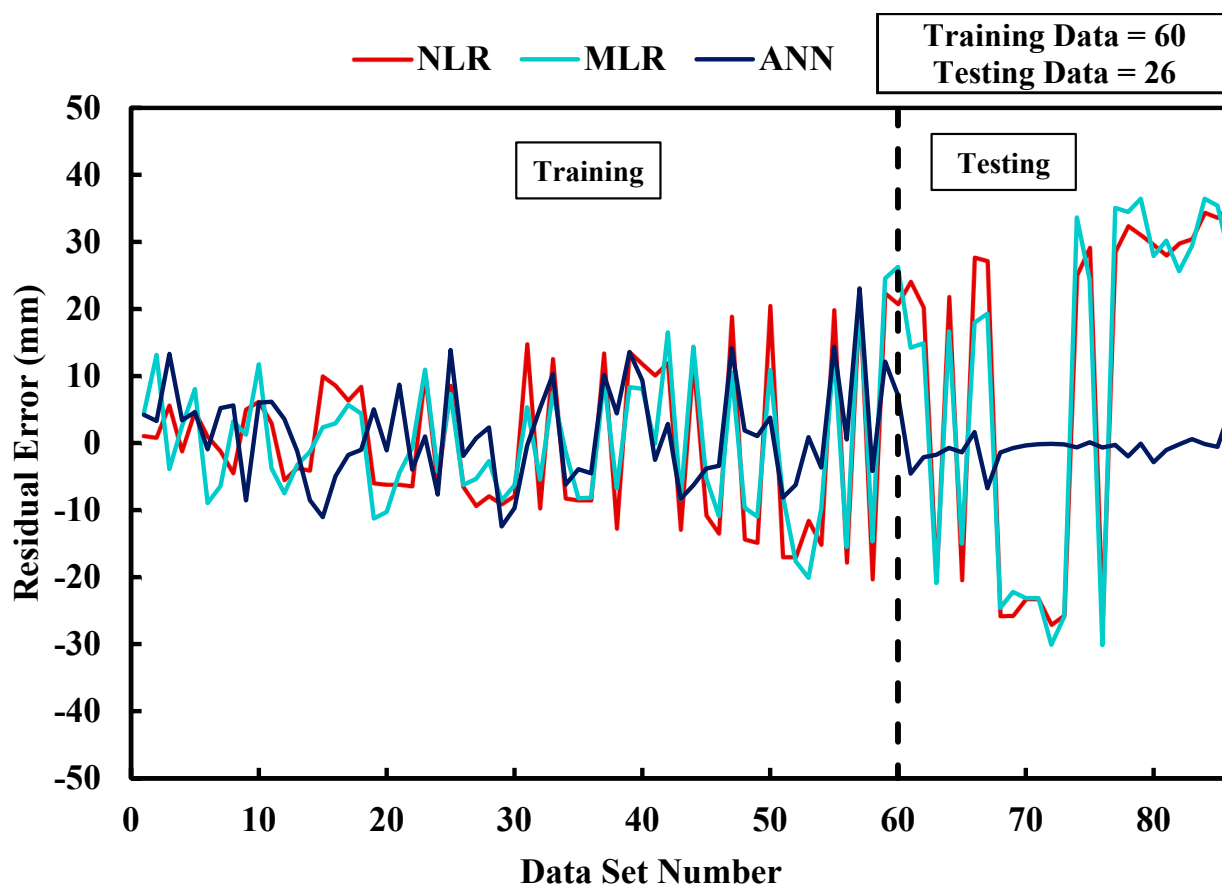
Figure 18. Comparison of the developed models using SI: (a) CS and (b) SL.

In addition, the created models were compared using residual error, as shown in Figure 19, for both the CS and SL predictions. The residual error value was obtained by subtracting the expected value from the measured value. The results of the CS prediction showed that the ANN model had the lowest error value, ranging from -23.0 to $+13.91$ MPa. The residual error for the NLR and MLR models ranged from -18.27 to 29.98 MPa and from -19.06 to 34.41 MPa, respectively. In contrast to the CS, the ANN model provided the lowest error value in the SL prediction. The error value was from -13.91 to 23.0 mm for the MLR model. The results of the NLR and ANN models were from -27.02 to 35.35 mm and from -30.13 to 36.46 mm, respectively.



(a)

Figure 19. Cont.

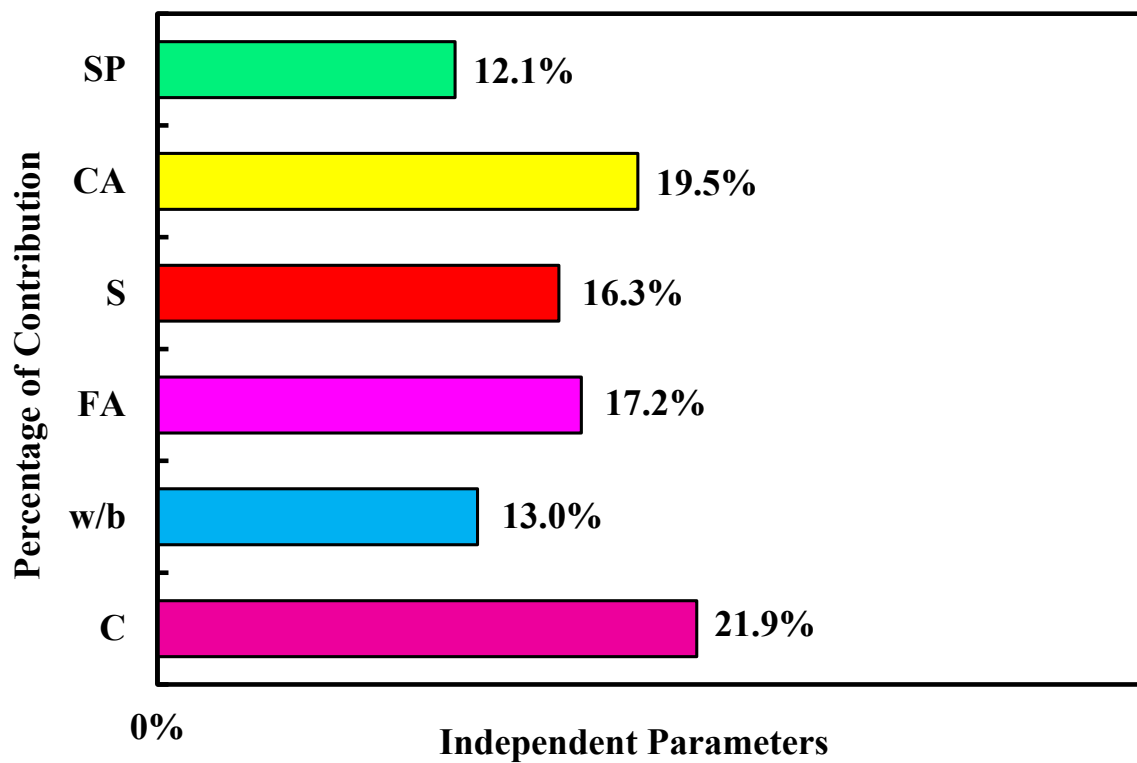


(b)

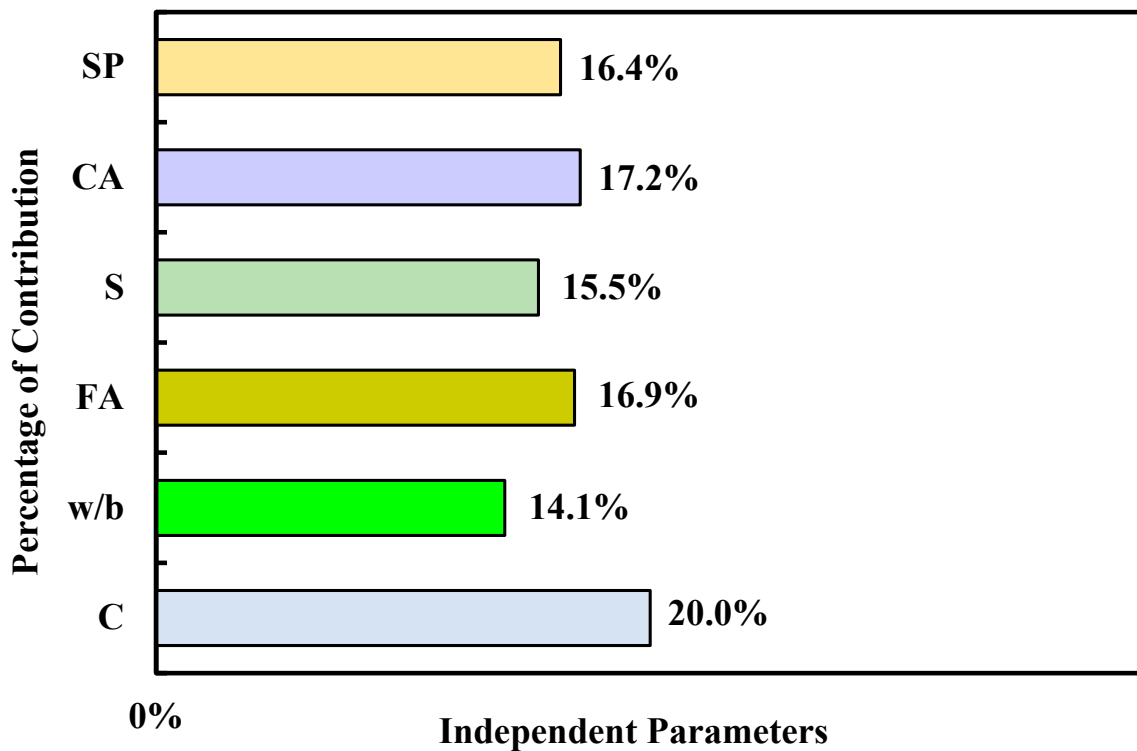
Figure 19. Variation between the measured and predicted (a) CS and (b) SL for the developed models based on the residual errors of NLR, MLR, and the ANN.

5. Sensitivity Investigation

Sensitivity analysis is an effective way to find and evaluate the effect of each independent variable on the modeled dependent variable, CS, and SL of fly ash-modified SCC [20]. For this purpose, the most accurate and efficient model was determined and selected for the analysis; in this study, the ANN was used for both CS and SL training datasets, as the analysis was performed for both collected data independently. During the sensitivity analysis, one parameter was excluded each time, and the assessment tools' results, such as R^2 , RMSE, and MAE, were independently calculated for each trial. The sensitivity results for CS and SL are shown in Table 5. The findings show that the cement content was the most effective parameter in predicting both CS and SL of SCC, followed by coarse aggregate and fly ash content (Figure 20).



(a)



(b)

Figure 20. The percentage contribution of input variables in predicting: (a) CS and (b) SL of FA-modified SCC using the ANN model.

Table 5. Sensitivity analysis results of the ANN model applied to the training dataset of FA-modified SCC for CS prediction.

Compressive strength	No.	Combination	Removed Parameter	R ²	RMSE (MPa)	MAE (MPa)	Ranking Based on RMSE and MAE
	1	C, w/b, FA, S, CA, SP	-	0.94	3.65	2.52	-
	2	w/b, FA, S, CA, SP	C	0.82	6.19	4.7	1
	3	C, FA, S, CA, SP	w/b	0.93	3.85	2.79	5
	4	C, w/b, S, CA, SP	FA	0.9	4.92	3.7	3
	5	C, w/b, FA, CA, SP	S	0.91	4.75	3.5	4
	6	C, w/b, FA, S, SP	CA	0.89	5.46	4.19	2
	7	C, w/b, FA, S, CA	SP	0.94	3.83	2.6	6
Slump flow diameter	No.	Combination	Removed Parameter	R ²	RMSE (mm)	MAE (mm)	Ranking based on RMSE and MAE
	1	C, w/b, FA, S, CA, SP	-	0.93	7.5	6	-
	2	w/b, FA, S, CA, SP	C	0.87	10.9	9.2	1
	3	C, FA, S, CA, SP	w/b	0.91	8.7	6.5	6
	4	C, w/b, S, CA, SP	FA	0.88	9.5	7.8	3
	5	C, w/b, FA, CA, SP	S	0.9	9	7.2	5
	6	C, w/b, FA, S, SP	CA	0.88	9.5	7.9	2
7	C, w/b, FA, S, CA	SP	0.9	9.4	7.6	4	

6. Conclusions

The current study aimed to find and propose an accurate and reliable model to predict self-compacted concrete's compressive strength and slump flow diameter modified with different fly ash types and quantities. Overall, 216 and 86 data samples for fly-ash-modified self-compacted concrete with different mixture proportions, cement content, water-to-binder ratio, sand content, coarse aggregate content, and superplasticizer dosage were collected from the literature. Based on the collected data and the results of three different model approaches, the following conclusions can be drawn:

1. The database for predicting CS included fly ash content ranging between 0 and 525 kg/m³, while that for predicting SL ranged between 0 and 468 kg/m³.
2. Increasing fly ash content caused an increase in the CS, but a lower impact was found on the SL. However, the impact of fly ash was found when the cement content was increased with an increase in the fly ash content simultaneously. It decreased the SL but increased the CS.
3. The compressive strength was more affected by aggregates rather than the slump flow. Increasing the CA and S content increased the CS but led to small changes in the SL. The influence of CA and S was noted to be higher at the maximum values of the variables. These findings highlight the importance of aggregates, specifically coarse and fine aggregates, in determining the compressive strength of concrete. Whereas

the slump flow, which measures the workability and fluidity of the mixture, did not substantially impact the CS, the composition and content of aggregates played a crucial role in enhancing the concrete's overall strength.

4. According to the various assessment criteria, such as R^2 , RMSE, and MAE, the ANN model was noted to have the highest accuracy and reliability for predicting both compressive strength and slump flow diameter of self-compacted concrete.
5. When predicting the CS, the ANN model had the highest R^2 of 0.94 for training and 0.95 for testing datasets. The lowest RMSE and MAE values were found to be 3.56 MPa and 2.54 MPa for training and 3.49 MPa and 2.45 MPa for testing datasets, respectively. However, in predicting the SL, the ANN model had an R^2 value of 0.93, RMSE of 7.5 mm, and MAE of 5.97 mm for the training dataset. The testing dataset's R^2 , RMSE, and MAE values were 0.997, 2.2 mm, and 1.39 mm, respectively.
6. Other statistical assessment tools, such as the OBJ function and SI value, were used. The ANN model maintained the lowest OBJ value of 3.12 and 5.5 for the CS and SL, respectively. Regarding the SI value, excellent performance was observed from the NLR model when predicting the CS, which was 0.10 for both the training and testing datasets. However, all models were observed to predict the SL. The SI value was 0.02 for both the NLR and MLR models and 0.01 for the ANN model.
7. The application of the Artificial Neural Network (ANN) model to different ranges of concrete strength (CS) and different classes of specimen length (SL) demonstrates its versatility and effectiveness. The higher CS strength range yielded more favorable outcomes, as indicated by an R^2 (coefficient of determination) value of 0.79, an RMSE (Root Mean Square Error) of 4.13 MPa, and an MAE (Mean Absolute Error) of 2.98 MPa. These metrics signify a strong correlation and relatively low prediction errors, suggesting the model performed well in estimating axial strength for high CS levels. Overall, the reported R^2 values demonstrated a good fit between the predicted and actual values, while the RMSE and MAE values indicated relatively small errors in the model's predictions. These findings suggest that the ANN model can effectively capture the relationships between the CS, SL, and axial strength, highlighting its potential as a reliable tool for estimating concrete strength in various scenarios and ranges.
8. Sensitivity analysis illustrates the cement content as the most effective parameter for both the CS and SL prediction of SCC.

7. Limitations and Future Work

1. Other soft computing models should be used to predict the slump flow diameter and compressive strength of the fly ash-based self-compacted concrete.
2. It is possible to assess other fly ash types and sources.
3. The prediction of other types of workability tests can be investigated.
4. Experiments need to be carried out to verify the produced models.
5. It is also important to determine the effect of fly ash content on flexural and tensile strength.

Funding: This research received no external funding.

Institutional Review Board Statement: Not applicable.

Informed Consent Statement: Not applicable.

Data Availability Statement: The data supporting the conclusions of this article are included with the article.

Conflicts of Interest: The author declares no conflict of interest.

References

1. Faraj, R.H.; Sherwani, A.F.H.; Daraei, A. Mechanical, fracture and durability properties of self-compacting high strength concrete containing recycled polypropylene plastic particles. *J. Build. Eng.* **2019**, *25*, 100808. [[CrossRef](#)]
2. Faraj, R.H.; Sherwani, A.F.H.; Jafer, L.H.; Ibrahim, D.F. Rheological behavior and fresh properties of self-compacting high strength concrete containing recycled PP particles with fly ash and silica fume blended. *J. Build. Eng.* **2020**, *34*, 101667. [[CrossRef](#)]
3. Faraj, R.H.; Ali, H.F.H.; Sherwani, A.F.H.; Hassan, B.R.; Karim, H. Use of recycled plastic in self-compacting concrete: A comprehensive review on fresh and mechanical properties. *J. Build. Eng.* **2020**, *30*, 101283. [[CrossRef](#)]
4. Deilami, S.; Aslani, F.; Elchalakani, M. An experimental study on the durability and strength of SCC incorporating FA, GGBS and MS. *Proc. Inst. Civ. Eng. Struct. Build.* **2019**, *172*, 327–339. [[CrossRef](#)]
5. Faraj, R.H.; Mohammed, A.A.; Mohammed, A.; Omer, K.M.; Ahmed, H.U. Systematic multiscale models to predict the compressive strength of self-compacting concretes modified with nanosilica at different curing ages. *Eng. Comput.* **2022**, *38* (Suppl. 3), 2365–2388. [[CrossRef](#)]
6. Neville, A.M.; Brooks, J.J. *Concrete Technology*; Longman Scientific & Technical: London, UK, 1987; pp. 242–246.
7. Neville, A.M. *Properties of Concrete*; Longman Scientific & Technical: London, UK, 1995; Volume 4.
8. Silvestre, J.; Silvestre, N.; De Brito, J. Review on concrete nanotechnology. *Eur. J. Environ. Civil. Eng.* **2016**, *20*, 455–485. [[CrossRef](#)]
9. Karamoozian, A.; Karamoozian, M.; Ashrafi, H. Effect of Nano Particles on Self Compacting Concrete: An Experimental Study. *Life Sci. J.* **2013**, *10*, 95–101.
10. Larsen, O.; Naruts, V.; Aleksandrova, O. Self-compacting concrete with recycled aggregates. *Mater. Today Proc.* **2019**, *19*, 2023–2026. [[CrossRef](#)]
11. Ghasemi, M.; Ghasemi, M.R.; Mousavi, S.R. Studying the fracture parameters and size effect of steel fiber-reinforced self-compacting concrete. *Constr. Build. Mater.* **2019**, *201*, 447–460. [[CrossRef](#)]
12. Ahmadi, M.A.; Alidoust, O.; Sadrinejad, I.; Nayeri, M. Development of mechanical properties of self compacting concrete contain rice husk ash. *Int. J. Comput. Inf. Syst. Sci. Eng.* **2007**, *1*, 259–262.
13. Dinakar, P.; Manu, S.N. Concrete mix design for high strength self-compacting concrete using metakaolin. *Mater. Des.* **2014**, *60*, 661–668. [[CrossRef](#)]
14. Güneyisi, E.; Gesoglu, M.; Al-Goody, A.; İpek, S. Fresh and rheological behavior of nano-silica and fly ash blended self-compacting concrete. *Constr. Build. Mater.* **2015**, *95*, 29–44. [[CrossRef](#)]
15. Madandoust, R.; Ranjbar, M.M.; Ghavidel, R.; Shahabi, S.F. Assessment of factors influencing mechanical properties of steel fiber reinforced self-compacting concrete. *Mater. Des.* **2015**, *83*, 284–294. [[CrossRef](#)]
16. Nikbin, I.M.; Beygi, M.H.A.; Kazemi, M.T.; Amiri, J.V.; Rahmani, E.; Rabbanifar, S.; Eslami, M. A comprehensive investigation into the effect of aging and coarse aggregate size and volume on mechanical properties of self-compacting concrete. *Mater. Des.* **2014**, *59*, 199–210. [[CrossRef](#)]
17. Mahmood, W.; Mohammed, A. Performance of ANN and M5P-tree to forecast the compressive strength of hand-mix cement-grouted sands modified with polymer using ASTM and BS standards and evaluate the outcomes using SI with OBJ assessments. *Neural Comput. Appl.* **2022**, *34*, 15031–15051. [[CrossRef](#)]
18. Asteris, P.G.; Lourenço, P.B.; Hajihassani, M.; Adami, C.-E.N.; Lemonis, M.E.; Skentou, A.D.; Marques, R.; Nguyen, H.; Rodrigues, H.; Varum, H. Soft computing based models for the prediction of masonry compressive strength. *Eng. Struct.* **2021**, *248*, 113276. [[CrossRef](#)]
19. Rahimi, I.; Gandomi, A.H.; Asteris, P.G.; Chen, F. Analysis and prediction of COVID-19 using sir, seiqr and machine learning models: Australia, italy and uk cases. *Information* **2021**, *12*, 109. [[CrossRef](#)]
20. Bardhan, A.; Gokceoglu, C.; Burman, A.; Samui, P.; Asteris, P.G. Efficient computational techniques for predicting the California bearing ratio of soil in soaked conditions. *Eng. Geol.* **2021**, *291*, 106239. [[CrossRef](#)]
21. Ahmed, H.U.; Mohammed, A.S.; Mohammed, A.A.; Faraj, R.H. Systematic multiscale models to predict the compressive strength of fly ash-based geopolymer concrete at various mixture proportions and curing regimes. *PLoS ONE* **2021**, *16*, e0253006. [[CrossRef](#)]
22. Koopialipoor, M.; Asteris, P.G.; Mohammed, A.S.; Alexakis, D.E.; Mamou, A.; Armaghani, D.J. Introducing stacking machine learning approaches for the prediction of rock deformation. *Transp. Geotech.* **2022**, *34*, 100756. [[CrossRef](#)]
23. Ahmed, H.U.; Mohammed, A.S.; Faraj, R.H.; Abdalla, A.A.; Qaidi, S.M.; Sor, N.H.; Mohammed, A.A. Innovative modeling techniques including MEP, ANN and FQ to forecast the compressive strength of geopolymer concrete modified with nanoparticles. *Neural Comput. Appl.* **2023**, *35*, 12453–12479. [[CrossRef](#)]
24. Asteris, P.G.; Ashrafian, A.; Rezaie-Balf, M. Prediction of the Compressive Strength of Self-Compacting Concrete using Surrogate Models. *Comput. Concr.* **2019**, *24*, 137–150.
25. Emad, W.; Mohammed, A.S.; Bras, A.; Asteris, P.G.; Kurda, R.; Muhammed, Z.; Hassan, A.M.; Qaidi, S.M.A.; Sihag, P. Meta-model techniques to estimate the compressive strength of UHPFRC using various mix proportions and a high range of curing temperatures. *Constr. Build. Mater.* **2022**, *349*, 128737. [[CrossRef](#)]
26. Mahmood, W.; Mohammed, A.S.; Asteris, P.G.; Kurda, R.; Armaghani, D.J. Modeling flexural and compressive strengths behaviour of cement-grouted sands modified with water reducer polymer. *Appl. Sci.* **2022**, *12*, 1016. [[CrossRef](#)]

27. Asteris, P.G.; Koopialipoor, M.; Armaghani, D.J.; Kotsonis, E.A.; Lourenço, P.B. Prediction of Cement-based Mortars Compressive Strength using Machine Learning Techniques. *Neural Comput. Appl.* **2021**, *33*, 13089–13121. [[CrossRef](#)]
28. Jaf, D.K.I.; Abdulrahman, P.I.; Abdulrahman, A.S.; Mohammed, A.S. Effitoned soft computing models to evaluate the impact of silicon dioxide (SiO₂) to calcium oxide (CaO) ratio in fly ash on the compressive strength of concrete. *J. Build. Eng.* **2023**, *74*, 106820.
29. Farooq, F.; Czarnecki, S.; Niewiadomski, P.; Aslam, F.; Alabduljabbar, H.; Ostrowski, K.A.; Śliwa-Wieczorek, K.; Nowobilski, T.; Malazdrewicz, S. A comparative study for the prediction of the compressive strength of self-compacting concrete modified with fly. *Materials* **2021**, *14*, 4934. [[CrossRef](#)]
30. Patel, R.; Hossain, K.M.A.; Shehata, M.; Bouzoubaa, N.; Lachemi, M. Development of statistical models for mixture design of high-volume fly ash self-consolidating concrete. *Mater. J.* **2004**, *101*, 294–302.
31. Ghezal, A.; Khayat, K.H. Optimizing self-consolidating concrete with limestone filler by using statistical factorial design methods. *Mater. J.* **2002**, *99*, 264–272.
32. Sonebi, M. Applications of statistical models in proportioning medium-strength self-consolidating concrete. *Mater. J.* **2004**, *101*, 339–346.
33. Sonebi, M. Medium strength self-compacting concrete containing fly ash: Modelling using factorial experimental plans. *Cem. Concr. Res.* **2004**, *34*, 1199–1208. [[CrossRef](#)]
34. Sukumar, B.; Nagamani, K.; Raghavan, R.S. Evaluation of strength at early ages of self-compacting concrete with high volume fly ash. *Constr. Build. Mater.* **2008**, *22*, 1394–1401. [[CrossRef](#)]
35. Bouzoubaa, N.; Lachemi, M. Self-compacting concrete incorporating high volumes of class F fly ash: Preliminary results. *Cem. Concr. Res.* **2001**, *31*, 413–420. [[CrossRef](#)]
36. Bui, V.K.; Akkaya, Y.; Shah, S.P. Rheological model for self-consolidating concrete. *Mater. J.* **2002**, *99*, 549–559.
37. Güneyisi, E.; Gesoğlu, M.; Özbay, E. Strength and drying shrinkage properties of self-compacting concretes incorporating multi-system blended mineral admixtures. *Constr. Build. Mater.* **2010**, *24*, 1878–1887. [[CrossRef](#)]
38. Pathak, N.; Siddique, R. Properties of self-compacting-concrete containing fly ash subjected to elevated temperatures. *Constr. Build. Mater.* **2012**, *30*, 274–280. [[CrossRef](#)]
39. Jalal, M.; Mansouri, E. Effects of fly ash and cement content on rheological, mechanical, and transport properties of high-performance self-compacting concrete. *Sci. Eng. Compos. Mater.* **2012**, *19*, 393–405. [[CrossRef](#)]
40. Dinakar, P.; Babu, K.G.; Santhanam, M. Mechanical properties of high-volume fly ash self-compacting concrete mixtures. *Struct. Concr.* **2008**, *9*, 109–116. [[CrossRef](#)]
41. Dinakar, P. Design of self-compacting concrete with fly ash. *Mag. Concr. Res.* **2012**, *64*, 401–409. [[CrossRef](#)]
42. Nehdi, M.; Pardhan, M.; Koshowski, S. Durability of self-consolidating concrete incorporating high-volume replacement composite cements. *Cem. Concr. Res.* **2004**, *34*, 2103–2112. [[CrossRef](#)]
43. Barbhuiya, S. Effects of fly ash and dolomite powder on the properties of self-compacting concrete. *Constr. Build. Mater.* **2011**, *25*, 3301–3305. [[CrossRef](#)]
44. Venkatakrishnaiah, R.; Sakthivel, G. Bulk utilization of flyash in self compacting concrete. *KSCE J. Civil. Eng.* **2015**, *19*, 2116–2120. [[CrossRef](#)]
45. Sun, Z.J.; Duan, W.W.; Tian, M.L.; Fang, Y.F. Experimental research on self-compacting concrete with different mixture ratio of fly ash. In *Advanced Materials Research*; Trans Tech Publications Ltd.: Bäch, Switzerland, 2011; Volume 236, pp. 490–495.
46. Ramanathan, P.; Baskar, I.; Muthupriya, P.; Venkatasubramani, R. Performance of self-compacting concrete containing different mineral admixtures. *KSCE J. Civil. Eng.* **2013**, *17*, 465–472. [[CrossRef](#)]
47. Boel, V.; Audenaert, K.; De Schutter, G.; Heirman, G.; Vandewalle, L.; Desmet, B.; Vantomme, J. Transport properties of self compacting concrete with limestone filler or fly ash. *Mater. Struct.* **2007**, *40*, 507–516. [[CrossRef](#)]
48. Douglas, R.P.; Bui, V.K.; Akkaya, Y.; Shah, S.P. Properties of Self-consolidating concrete containing class f fly ash: With a Verification of the minimum paste volume method. *Spec. Publ.* **2006**, *233*, 45–64.
49. Bingöl, A.F.; Tohumcu, İ. Effects of different curing regimes on the compressive strength properties of self compacting concrete incorporating fly ash and silica fume. *Mater. Des.* **2013**, *51*, 12–18. [[CrossRef](#)]
50. Hemalatha, T.; Ramaswamy, A.; Chandra Kishen, J.M. Micromechanical analysis of self compacting concrete. *Mater. Struct.* **2015**, *48*, 3719–3734. [[CrossRef](#)]
51. Krishnapal, P.; Yadav, R.K.; Rajeev, C. Strength characteristics of self compacting concrete containing fly ash. *Res. J. Eng. Sci. ISSN* **2013**, *2278*, 9472.
52. Dhiyaneshwaran, S.; Ramanathan, P.; Baskar, I.; Venkatasubramani, R. Study on durability characteristics of self-compacting concrete with fly ash. *Jordan J. Civ. Eng.* **2013**, *7*, 342–353.
53. Siddique, R. Properties of self-compacting concrete containing class F fly ash. *Mater. Des.* **2011**, *32*, 1501–1507. [[CrossRef](#)]
54. Mahalingam, B.; Nagamani, K. Effect of processed fly ash on fresh and hardened properties of self compacting concrete. *Int. J. Earth Sci. Eng.* **2011**, *4*, 930–940.
55. Muthupriya, P.; Sri, P.N.; Ramanathan, M.P.; Venkatasubramani, R. Strength and workability character of self compacting concrete with GGBFS, FA and SF. *Int. J. Emerg. Trends Eng. Dev.* **2012**, *2*, 424–434.

56. Siddique, R.; Aggarwal, P.; Aggarwal, Y. Influence of water/powder ratio on strength properties of self-compacting concrete containing coal fly ash and bottom ash. *Constr. Build. Mater.* **2012**, *29*, 73–81. [[CrossRef](#)]
57. Gesoğlu, M.; Güneyisi, E.; Özbay, E. Properties of self-compacting concretes made with binary, ternary, and quaternary cementitious blends of fly ash, blast furnace slag, and silica fume. *Constr. Build. Mater.* **2009**, *23*, 1847–1854. [[CrossRef](#)]
58. Nepomuceno, M.C.; Pereira-de-Oliveira, L.A.; Lopes, S.M.R. Methodology for the mix design of self-compacting concrete using different mineral additions in binary blends of powders. *Constr. Build. Mater.* **2014**, *64*, 82–94. [[CrossRef](#)]
59. Gettu, R.; Izquierdo, J.; Gomes, P.C.C.; Josa, A. Development of high-strength self-compacting concrete with fly ash: A four-step experimental methodology. In Proceedings of the 27th Conference on Our World in Concrete & Structures, Singapore, 29–30 August 2002; Tam, C.T., Ho, D.W., Paramasivam, P., Tan, T.H., Eds.; Premier Pte. Ltd.: Singapore, 2002; pp. 217–224.
60. Şahmaran, M.; Yaman, İ.Ö.; Tokyay, M. Transport and mechanical properties of self consolidating concrete with high volume fly ash. *Cem. Concr. Compos.* **2009**, *31*, 99–106. [[CrossRef](#)]
61. Liu, M. Self-compacting concrete with different levels of pulverized fuel ash. *Constr. Build. Mater.* **2010**, *24*, 1245–1252. [[CrossRef](#)]
62. Piro, N.S.; Mohammed, A.S.; Hamad, S.M.; Kurda, R.; Qader, B.S. Multifunctional computational models to predict the long-term compressive strength of concrete incorporated with waste steel slag. *Struct. Concr.* **2023**, *24*, 2093–2112. [[CrossRef](#)]
63. Piro, N.S.; Mohammed, A.; Hamad, S.M.; Kurda, R. Artificial neural networks (ANN), MARS, and adaptive network-based fuzzy inference system (ANFIS) to predict the stress at the failure of concrete with waste steel slag coarse aggregate replacement. *Neural Comput. Appl.* **2023**, *35*, 13293–13319. [[CrossRef](#)]
64. Ibrahim, A.K.; Dahir, H.Y.; Mohammed, A.S.; Omar, H.A.; Sedo, A.H. The effectiveness of surrogate models in predicting the long-term behavior of varying compressive strength ranges of recycled concrete aggregate for a variety of shapes and sizes of specimens. *Arch. Civil. Mech. Eng.* **2023**, *23*, 61. [[CrossRef](#)]
65. Ahmed, A.; Abubakr, P.; Mohammed, A.S. Efficient models to evaluate the effect of C3S, C2S, C3A, and C4AF contents on the long-term compressive strength of cement paste. *Structures* **2023**, *47*, 1459–1475. [[CrossRef](#)]
66. Mohammed, A.; Rafiq, S.; Sihag, P.; Mahmood, W.; Ghafor, K.; Sarwar, W. ANN, M5P-tree model, and nonlinear regression approaches to predict the compression strength of cement-based mortar modified by quicklime at various water/cement ratios and curing times. *Arab. J. Geosci.* **2020**, *13*, 1216. [[CrossRef](#)]
67. Mohammed, A.; Rafiq, S.; Sihag, P.; Kurda, R.; Mahmood, W. Soft computing techniques: Systematic multiscale models to predict the compressive strength of HVFA concrete based on mix proportions and curing times. *J. Build. Eng.* **2021**, *33*, 101851. [[CrossRef](#)]
68. Mohammed, A.S.; Emad, W.; Sarwar Qadir, W.; Kurda, R.; Ghafor, K.; Kadhim Faris, R. Modeling the Impact of Liquid Polymers on Concrete Stability in Terms of a Slump and Compressive Strength. *Appl. Sci.* **2023**, *13*, 1208. [[CrossRef](#)]
69. Ali, R.; Muayad, M.; Mohammed, A.S.; Asteris, P.G. Analysis and prediction of the effect of Nanosilica on the compressive strength of concrete with different mix proportions and specimen sizes using various numerical approaches. *Struct. Concr.* **2022**, *24*, 4161–4184. [[CrossRef](#)]
70. Abdalla, A.; Mohammed, A.S. Hybrid MARS-, MEP-, and ANN-based prediction for modeling the compressive strength of cement mortar with various sand size and clay mineral metakaolin content. *Arch. Civil. Mech. Eng.* **2022**, *22*, 194. [[CrossRef](#)]
71. Asteris, P.G.; Nozhati, S.; Nikoo, M.; Cavaleri, L.; Nikoo, M. Krill herd algorithm-based neural network in structural seismic reliability evaluation. *Mech. Adv. Mater. Struct.* **2019**, *26*, 1146–1153. [[CrossRef](#)]
72. Asteris, P.G.; Lemonis, M.E.; Le, T.-T.; Tsavdaridis, K.D. Evaluation of the ultimate eccentric load of rectangular CFSTs using advanced neural network modeling. *Eng. Struct.* **2021**, *248*, 113297. [[CrossRef](#)]
73. Asteris, P.G.; Lourenço, P.B.; Adami, C.A.; Roussis, P.C.; Armaghani, D.J.; Cavaleri, L.; Chalioris, C.E.; Hajihassani, M.; Lemonis, M.E.; Mohammed, A.S.; et al. Revealing the nature of metakaolin-based concrete materials using Artificial Intelligence Techniques. *Constr. Build. Mater.* **2022**, *322*, 126500. [[CrossRef](#)]
74. Asteris, P.G.; Armaghani, D.J.; Hatzigeorgiou, G.D.; Karayannis, C.G.; Pilakoutas, K. Predicting the shear strength of reinforced concrete beams using Artificial Neural Networks. *Computers and Concrete. An. Int. J.* **2019**, *24*, 469–488.
75. Armaghani, D.J.; Asteris, P.G. A comparative study of ANN and ANFIS models for the prediction of cement-based mortar materials compressive strength. *Neural Comput. Appl.* **2021**, *33*, 4501–4532. [[CrossRef](#)]
76. Mohammed, A.; Kurda, R.; Armaghani, D.J.; Hasanipanah, M. Prediction of compressive strength of concrete modified with fly ash: Applications of neuro-swarm and neuro-imperialism models. *Comput. Concr.* **2021**, *27*, 489.
77. Qadir, W.; Ghafor, K.; Mohammed, A. Evaluation the effect of lime on the plastic and hardened properties of cement mortar and quantified using Vipulanandan model. *Open Eng.* **2019**, *9*, 468–480. [[CrossRef](#)]
78. Sarwar, W.; Ghafor, K.; Mohammed, A. Regression analysis and Vipulanandan model to quantify the effect of polymers on the plastic and hardened properties with the tensile bonding strength of the cement mortar. *Results Mater.* **2019**, *1*, 100011. [[CrossRef](#)]
79. Qaidi, S.; Al-Kamaki, Y.S.; Al-Mahaidi, R.; Mohammed, A.S.; Ahmed, H.U.; Zaid, O.; Althoey, F.; Ahmad, J.; Isleem, H.F.; Bennetts, I. Investigation of the effectiveness of CFRP strengthening of concrete made with recycled waste PET fine plastic aggregate. *PLoS ONE* **2022**, *17*, e0269664. [[CrossRef](#)]
80. Abdalla, A.A.; Salih Mohammed, A. Theoretical models to evaluate the effect of SiO₂ and CaO contents on the long-term compressive strength of cement mortar modified with cement kiln dust (CKD). *Arch. Civ. Mech. Eng.* **2022**, *22*, 105. [[CrossRef](#)]

81. Barkhordari, M.S.; Armaghani, D.J.; Mohammed, A.S.; Ulrikh, D.V. Data-driven compressive strength prediction of fly ash concrete using ensemble learner algorithms. *Buildings* **2022**, *12*, 132. [[CrossRef](#)]
82. Piro, N.S.; Salih, A.; Hamad, S.M.; Kurda, R. Comprehensive multiscale techniques to estimate the compressive strength of concrete incorporated with carbon nanotubes at various curing times and mix proportions. *J. Mater. Res. Technol.* **2021**, *15*, 6506–6527. [[CrossRef](#)]

Disclaimer/Publisher's Note: The statements, opinions and data contained in all publications are solely those of the individual author(s) and contributor(s) and not of MDPI and/or the editor(s). MDPI and/or the editor(s) disclaim responsibility for any injury to people or property resulting from any ideas, methods, instructions or products referred to in the content.